nature communications

Article

https://doi.org/10.1038/s41467-025-63581-1

Mechano-crosstalk between living and artificial cells

Received: 26 March 2024

Accepted: 22 August 2025

Published online: 29 September 2025

Check for updates

Xiaolei Yu[1], Vincent Mukwaya[1], Li Wang[2], Weili Zhao[2], Stephen Mann[1,3,4] ✉ & Hongjing Dou[1] ✉

The mechanisms underlying the probing and response of cells to direct cell-presented mechanical signals generated in the local microenvironment are important controllers of diverse cell behaviours. Here we construct a model artificial pathogen cell with the similar compartmentalization architecture and same range of tunable rigidity as found in natural cells. By incubating the artificial cells with macrophages, we investigate the mechanisms of mechano-crosstalk between living cells and model protocells. We show that macrophages are equipped with distinct pseudopodia that facilitate the probing of cell-presented mechanical signals. Increasing the rigidity of the artificial pathogen cells enhances the proinflammatory polarization of the macrophages by promoting the docking of the mechanosensitive molecular clutch, actin assembly, and pseudopodia extension. The relationship between cell morphology and functional plasticity involves a mechano-transduction axis including artificial cell rigidity, pseudopodia, and macrophage inflammatory response. Taken together, our model protocells provide a new platform to decouple cell-presented mechanical signals and highlight their role in governing protocell-living cell mechano-crosstalk.

Extensive research has been undertaken to reveal and understand the role of biophysical cues in the microenvironment as essential controllers of cell behaviors via processes of mechano-sensing and mechano-transduction[1–4]. Consequently, tailoring the biophysical properties of biomaterials is a predominant strategy for exploring cell-microenvironment interactions and regulating the fate of cells in biomedical applications[5,6]. In particular, extracellular matrix (ECM)-mimicking materials have been extensively designed with tunable rigidity, viscoelasticity, degradability, topography, and dynamic cues[5,7]. However, decoupling the confounding biophysical parameters remains challenging such that the rational design and programmable control of cell-cell mechano-transduction is still in its infancy[8].

Individual cells can exhibit changes in mechanical properties during their lifetime; for example, the stiffness of breast cancer cells is lower than that of normal cells[9]; the modulus of human red blood cells increases during the aging process[10]; and the stiffness at the local cell surface area of mycobacteria exhibits a significant and consistent increase prior to its division[11]. An underlying question is how the physiological or pathological roles relate to such mechanical changes. To date, most studies in mechano-transduction have been performed on low-motile tissue cells with highly polymerized actin organization[12–16]. Immune cells, including macrophages, exhibit a highly active migratory capacity[17]. Macrophages scan and transit between individual cells, and implement distinct dynamic functions that involve dynamical cytoskeletal reorganization, and which are dependent on their pro-inflammatory or anti-inflammatory polarization states[18]. They also come into contact with hematopoietic stem cells, determine hematopoietic clonality by monitoring stem cell

[1]State Key Laboratory of Metal Matrix Composites, School of Materials Science and Engineering, Shanghai Jiao Tong University, Shanghai, P. R. China. [2]Shanghai Institute of Hematology, State Key Laboratory of Medical Genomics, National Research Center for Translational Medicine at Shanghai, Ruijin Hospital affiliated to Shanghai Jiao Tong University School of Medicine, Shanghai, China. [3]Centre for Protolife Research and Centre for Organized Matter Chemistry, School of Chemistry, University of Bristol, Bristol, UK. [4]Max Planck-Bristol Centre for Minimal Biology, School of Chemistry, University of Bristol, Bristol, UK. ✉e-mail: s.mann@bristol.ac.uk; hjdou@sjtu.edu.cn

quality[19]; bind with lymphocytes (T cells, B cells, and NK cells), and form immunological synapses to stimulate specific expansion and differentiation[20–23]. However, knowledge regarding macrophage mechano-crosstalk and functional plasticity is currently limited to how factors presented by ECM-mimicking materials or microparticles influence cellular polarization, lacking a context that mimics direct cell-cell interactions[24–28].

As cellular behavior is profoundly altered when cells are cultured in diverse physiological microenvironments, a comprehensive mechanistic understanding of the interplay between macrophage polarization and cell-presented mechanical signals requires a combination of different sets of materials that complement each other[7,29,30]. To address this, here we construct an artificial pathogen cell (Art-P cell) model with a similar compartmentalization architecture and same range of tunable rigidity as is found in natural cells, and use the protocells to investigate macrophage mechano-sensing and -transduction in response to cell-presented signals. We demonstrate that macrophages are equipped with pseudopodia that facilitate their probing when the rigidity of the Art-P cells induces a cellular response. Increasing the rigidity of the Art-P cells promotes the docking of a mechanosensitive molecular clutch, thereby establishing a linkage between the artificial cell membrane and cytoskeleton. The resulting enhanced polymerization of the cytoskeleton increases the robustness of the pseudopodia and induces pro-inflammatory polarization of the macrophages, forming a distinct mechano-transduction axis of artificial cell rigidity-pseudopodia-inflammatory response. We demonstrate the involvement of ion channels Piezo1 and RhoA/ROCK signaling in the axis, representing two distinct mechano-activation strategies. Taken together, our study provides insight into the mechanism and function of mechanical signals that influence the inflammatory response of the macrophages during protocell-cell interactions, thus providing valuable insights for the rational design and development of advanced immunomodulatory biomaterials.

Results

Artificial cells with tunable cytomimetic rigidity initiate macrophage cytoskeletal reorganization

Inspired by the central roles played by carbohydrates in the mediation of cell-cell interactions, we constructed artificial cell-like membrane-bounded polysaccharide-based architectures (polysaccharidosomes)[31] (Fig. 1a). The polysaccharidosomes were prepared by a three-step process: (i) doping of carboxymethyl dextran (Dex-COOH; M_w = 1,500 Da) into $CaCO_3$ microparticles to generate negatively-charged colloidal templates for membrane assembly (Fig. 1b); (ii) electrostatically driven assembly of aminated hyaluronic acid (HA-NH_2; M_w = 40 kDa; positively charged) at the surface of the negatively charged $CaCO_3$ particles, and (iii) crosslinking of the assembled HA-NH_2 membrane and dissolution of the $CaCO_3$ core. We selected hyaluronic acid as a building block due to its presence on the outer surface of cells, where it serves as a key component of glycocalyx—a dense layer of intricate polysaccharide complex on the cell surface with more than 20 nm thickness[32,33]. Additionally, we considered its affinity for CD44, a cell-surface glycoprotein that is involved in cell-cell adhesion and interactions[34]. HA and Dex were functionalized via previously reported procedures[31] (Supplementary Figs. 1, 2). We chose PEG-bis(*N*-succinimidyl succinate, PEG-Succ) (M_w = 2,000 Da) as a crosslinker to passivate the surface of the polysaccharidosome membrane, and to prevent non-specific cell adhesion and adsorption of proteins from the culture medium[13].

Fluorescence labeling of the HA-NH_2 membrane confirmed that the water-filled hollow polysaccharidosomes were uniform in size (diameter = 25.67 ± 2.5 μm, Supplementary Fig. 3), and produced in high yield (Fig. 1c, d). To modulate the rigidity of the artificial cells while ensuring that the surface properties remained unchanged, we trapped sodium alginate (SA) within the preformed polysaccharidosomes. To achieve this, we increased the permeability of the polysaccharidosomes to SA by using urea to disrupt the intermolecular hydrogen bonding network of the crosslinked HA-NH_2 membrane, followed by removal of urea and concomitant contraction of the membrane pores and trapping of the sequestered SA[35,36] (Fig. 1e, Supplementary Fig. 4). By using different SA concentrations, soft (no SA), medium-rigid (SA = 5 mg/mL, medium), and rigid (SA = 15 mg/mL) polysaccharidosomes were prepared with a greater resistance to collapse after air-drying or changes in osmotic pressure being achieved as the level of trapped SA was increased (Fig. 1f–h and Supplementary Figs. 5, 6). Corresponding fluorescence line profiles indicated that the polysaccharidosomes were internally filled with different amounts of fluorescently labeled SA, while maintaining their structural integrity and surface properties (Fig. 1g, Supplementary Figs. 7, 8; Supplementary Movies 1–3). As cells often probe the mechanical feedback of their local surroundings on a micrometer scale[37], we performed an atomic force microscopy (AFM) characterization of the Young's modulus of the polysaccharidosomes in the aqueous phase using a 12 μm diameter spherical probe. The Young's moduli of the soft, medium and rigid polysaccharidosomes were 1.01 ± 0.47, 2.37 ± 1.06, and 5.98 ± 2.40 kPa, respectively (Fig. 1i). Notably, the moduli of the polysaccharidosomes were within the range of values determined for natural cells[3,9,11].

To determine whether macrophages can sense and respond to mechanical cues presented by the polysaccharidosome membrane, we cultured macrophages (RAW264.7 cells) with soft, medium, or rigid polysaccharidosomes for periods of 24 h. Independent of protocell rigidity, the polysaccharidosomes and macrophages were often observed in close contact (Supplementary Fig. 9a), enhanced levels of filamentous actin (F-actin) were localized within the macrophages at the contact junctions (Supplementary Fig. 9b), and a slight deformation of the polysaccharidosome membrane occurred at the contact interface (Supplementary Fig. 9c). As the contractible actin cytoskeleton is a mechanical sensor and accumulates at regions of high tension[38], the results suggested that the macrophages responded mechanically on contact with the artificial cells, possibly as a reaction to the elastic forces associated with the polysaccharidosome membrane.

As macrophages implement distinct dynamic functions that are dependent on the activation of polarization[18,24,26,39], and reorganization of the cytoskeleton leads to changes in cell spreading area[15], we first characterized the spreading area of the macrophages by F-actin staining of the cytoskeleton and found that the macrophages had a larger spreading area when cultured with soft polysaccharidosomes compared with their more rigid counterparts (Fig. 1j, k). The results indicated that mechanical cues from the polysaccharidosomes could initiate cytoskeletal reorganization in the macrophages. To determine whether protocell rigidity could activate macrophage polarization, we evaluated typical polarization markers (pro-inflammatory markers and anti-inflammatory marker) for macrophages cultured in the presence of polysaccharidosomes with different levels of rigidity (Supplementary Fig. 10a–d, Supplementary Table 1). In each case, there were no statistical differences in the expression of biological markers. The results indicated that there was no significant activation of macrophage polarization on contact with the soft, medium, or rigid polysaccharidosomes.

Rigid artificial pathogen cells promote pro-inflammatory polarization of macrophages

The above results indicated that macrophages sense and respond to mechanical cues presented by the polysaccharidosomes through cytoskeletal reorganization. Although the soft polysaccharidosomes induced increased cell spreading behavior, this enhancement was not sufficient to activate a polarization response in the macrophages. Previous studies have revealed that juxtacrine signaling and cell-cell interactions in immunocytes are orchestrated by multiple adhesion

https://doi.org/10.1038/s41467-025-63581-1

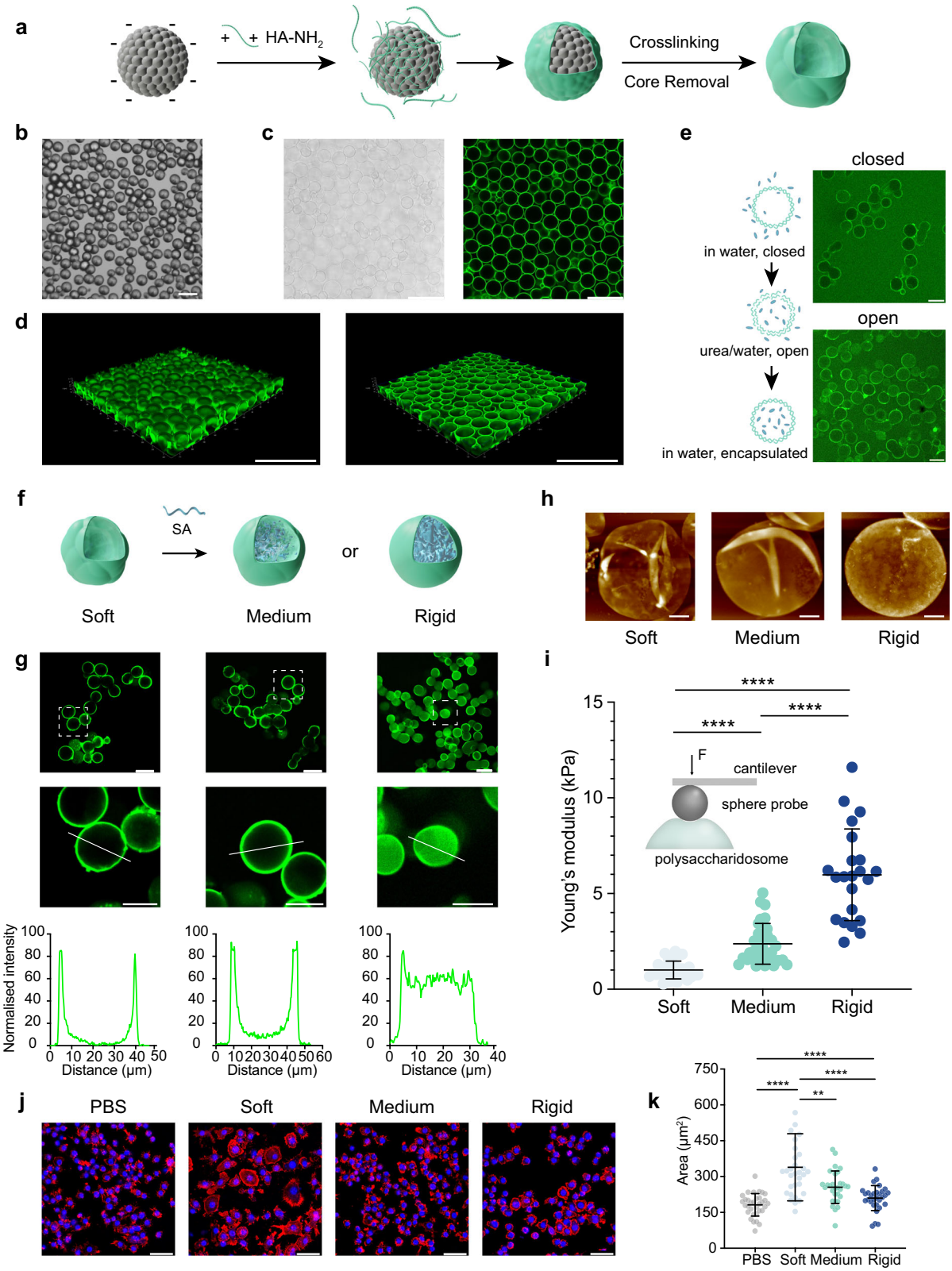

and regulatory molecules[40]. For example, both NK cells and T cells integrate synergistic signals from combinations of receptors to activate the immune response[41]. In living organisms, macrophages recognize pathogens such as bacteria, fungi, and parasites through specific receptors, thereby initiating their classical polarization. Besides directly killing the pathogen through phagocytosis, macrophages recruit other immunocytes to the infection site and activate adaptive immunity. The multifaceted functions make macrophages crucial targets for a wide range of human diseases[42]. These observations suggest that the mechanical cues presented by the polysaccharidosomes require a combination of biochemical signals to induce macrophage polarization. To achieve this, we covalently attached a potent pro-inflammatory activator (Pam3CSK4) to the polysaccharidosome membrane. Pam3CSK4 mimics the pathogen-

Fig. 1 | Construction, characterization, and interaction of polysaccharidosomes with macrophages. a Scheme depicting the fabrication route leading to the hollow polysaccharidosomes. Templates are coated with HA-NH_2, and then covalently crosslinked to form a continuous polysaccharide shell. The removal of templates yields intact polysaccharidosomes. **b** Optical microscopy image of $CaCO_3$ templates. Scale bar = 75 μm. **c** Confocal microscopy images of water-filled polysaccharidosomes after template dissolution. Scale bars = 50 μm. **d** Reconstructed 3D fluorescence images showing the intact (left) and clipped (right) structure of polysaccharidosomes (green: FITC-labeled HA-NH_2 membrane). Scale bars = 100 μm. **e** Scheme (left) and confocal microscopy images (right) showing the permeation and encapsulation of SA into polysaccharidosomes via a post-filling approach. Polysaccharidosomes are impermeable to SA in water (top right, closed). Adding urea increases the membrane permeability, allowing SA infusion (bottom right, open). Green: 5-AF labeled SA. Scale bars = 50 μm. **f** Scheme showing the preparation of polysaccharidosomes with tunable rigidity via filling with different concentrations of SA. **g** Confocal microscopy images of soft, medium, and rigid polysaccharidosomes with varying SA content, and corresponding normalized fluorescence intensity profiles of FITC-HA-NH_2 (green) and 5-AF-SA (green) across single polysaccharidosomes. Scale bars = 50 μm (enlarged, 25 μm). **h** AFM images of soft, medium, and rigid polysaccharidosomes after air-drying (scale bars = 5 μm). **i** Young's modulus of soft, medium, and rigid polysaccharidosomes (data are mean ± s.d., soft, $n = 31$; medium, $n = 32$; rigid, $n = 22$, three technical replicates). $^{****}P < 0.0001$. **j** Confocal microscopy images (red, F-actin; blue, nucleus; scale bars = 50 μm) and **k**, the relative quantification data of cell spreading area after incubation of the macrophages with the control sample (PBS), soft, medium, or rigid polysaccharidosomes for 24 h (data are mean ± s.d., control, $n = 33$; soft, 31; medium, 30; rigid, 30; three biological replicates) $^{****}P < 0.0001$, $^{**}P = 0.0045$. In **i**, **k** significance was determined by significance was determined by one-way ANOVA followed by Tukey's multiple comparison test. Source data are provided as a Source Data file.

associated molecular patterns (PAMPs) and is recognized by the toll-like receptor 1 (TLR1)/TLR2 receptors on macrophages[43]. As this type of signaling is commonly found on natural pathogens, we refer to the modified polysaccharidosomes as artificial pathogen cells (Art-P cells).

We attached Pam3CSK4 to the crosslinked HA-NH_2 membrane prior to template removal, followed by dissolution of the $CaCO_3$ core and uptake/retention of SA to produce soft, medium or rigid Art-P cells (Fig. 2a). The functionalization strategy employed ensured consistent attachment of Pam3CSK4 onto the Art-P cell surface, regardless of changes in rigidity. Moreover, the membrane-cytoplasm architecture enables membrane-specific functionalization of the ligands, providing a platform for studying the membrane signal-mediated intercellular interactions. The attachment of Pam3CSK4 resulted in a comparable increase in membrane roughness among different Art-P cells (Fig. 2b). The confirmation was further strengthened through surface fluorescence staining of Pam3CSK4 (Fig. 2c, d, Supplementary Fig. 11). Six different macrophage pro-inflammatory markers, including the gene expression of cytokines TNF-α, CCL4, IL-1β, and iNOS, the membrane receptor CD86, as well as the cellular secretion of nitric oxide, were evaluated after co-culturing with Art-P cells of different rigidity (Fig. 2e–g). Significantly, progressive increases in expression/secretion of each marker were observed as the rigidity of the Pam3CSK4-modified polysaccharidosomes was increased, indicating enhanced pro-inflammatory macrophage polarization. Control experiments with SA alone exhibited only low immunogenicity (Supplementary Fig. 12).

The above results suggest that increased chemo-mechanical coupling between the macrophages and Art-P cells with increased stiffness strongly influences immune function. As polarization is a downstream function of cell mechano-sensing, we investigated the changes in cytoskeletal polymerization preceding the different immune responses. Measurements of the degree of cytoskeletal polymerization in the macrophages showed an increase in F-actin assembly after incubation with more rigid Art-P cells (Fig. 2h). The changes in the cytoskeleton induced by the mechanical signals were validated through visualization of the F-actin structure, which showed that the resting macrophages consisted of a cortical F-actin cytoskeleton and sub-membranous stratum, and that interaction with the Art-P cells resulted in symmetry-breaking morphological changes (Fig. 2j). Specifically, the increase in Art-P cell rigidity led to the generation of punctate actin assemblies by macrophages, which served as local stress points, and gradually developed into organized actin stress fibers. These fibers exhibited enhanced alignment as quantified by fiber anisotropy (Fig. 2i). The highly aligned actin filament network suggested enhanced cytoskeletal integrity and cytoskeletal tension[38]. Thus, the rigid Art-P cells could positively promote the generation of intracellular forces.

Taken together, our results indicate that mechanical cues presented by protocells require biochemical cues to effectively regulate macrophage pro-inflammatory polarization. The inflammatory response increases considerably when the Young's modulus of the Art-P cells is increased from approximately 1.0 to 6.0 kPa. Additionally, the increase in rigidity facilitates the assembly of stress fibers in macrophages. Because pro-inflammatory polarization is closely associated with cytoskeletal reorganization, we conjecture that the enhanced intracellular tension, as evidenced by the assembly of organized stress fibers, might also be coupled to the increased immune response.

Macrophages extend robust pseudopodia to anchor onto rigid artificial pathogen cells

Given the above observations, we conducted an in-depth investigation of the mechano-transmission process associated with macrophage/Art-P cell contact-dependent interactions. Initially, our focus was directed towards the interface between living cells and protocells. 3D representative confocal images and quantitative analysis by flow cytometry revealed a significant increase in macrophage adhesion on the rigid Art-P cells after 24 h compared to the softer counterparts (Supplementary Fig. 14). The relatively stiff cell nuclei in both groups also showed noticeable deformation, suggesting that the mechanical cues could be transmitted into the nucleus[44–46] (Fig. 3a).

To investigate the macrophage/Art-P cell interface with enhanced clarity, we employed transmission electron microscopy (TEM) imaging (Fig. 3b, c). Intriguingly, the macrophages displayed distinct contact mechanisms with Art-P cells of varying rigidity. Specifically, the macrophages extended pseudopodia to probe the Art-P cell membrane, with a more rigid interface associated with increasing numbers of robust pseudopodia that could penetrate the polysaccharidosome membrane. Based on the structural differences, we further quantified the width of the pseudopodia on soft versus rigid interfaces, revealing a significantly thinner morphology on rigid interfaces (Fig. 3d). Furthermore, the macrophages lacked large lamellipodia, slender filopodia and micro-tentacles that are typically observed on 2D and 3D substrates[47] (Supplementary Fig. 15). The robust pseudopodia are nano-cylindrical structures that are known to respond to local environmental cues with ultrahigh sensitivity[48]. Notably, similar membrane protrusions were also observed to act as a macrophage mechano-sensor during the uptake of nanoparticles[4]. The spatial arrangement of rigidity-induced pseudopodia was further elucidated by the 3D landscape of the actin structure (Fig. 3e, Supplementary Movies. 4, 5). These robust yet slender pseudopodia were fully extended and actively engaged in exhaustive interactions with the rigid Art-P cells.

Pathogens of living cells exhibit considerable variations in size, ranging from microscopic to macroscopic scales. Macrophages possess the ability to directly eliminate small pathogens through phagocytosis (typically less than 10 μm), while they also function as secretory cells for generating pathogen-induced damage and recruiting other immune cells upon recognition of larger pathogens[49]. To further

https://doi.org/10.1038/s41467-025-63581-1

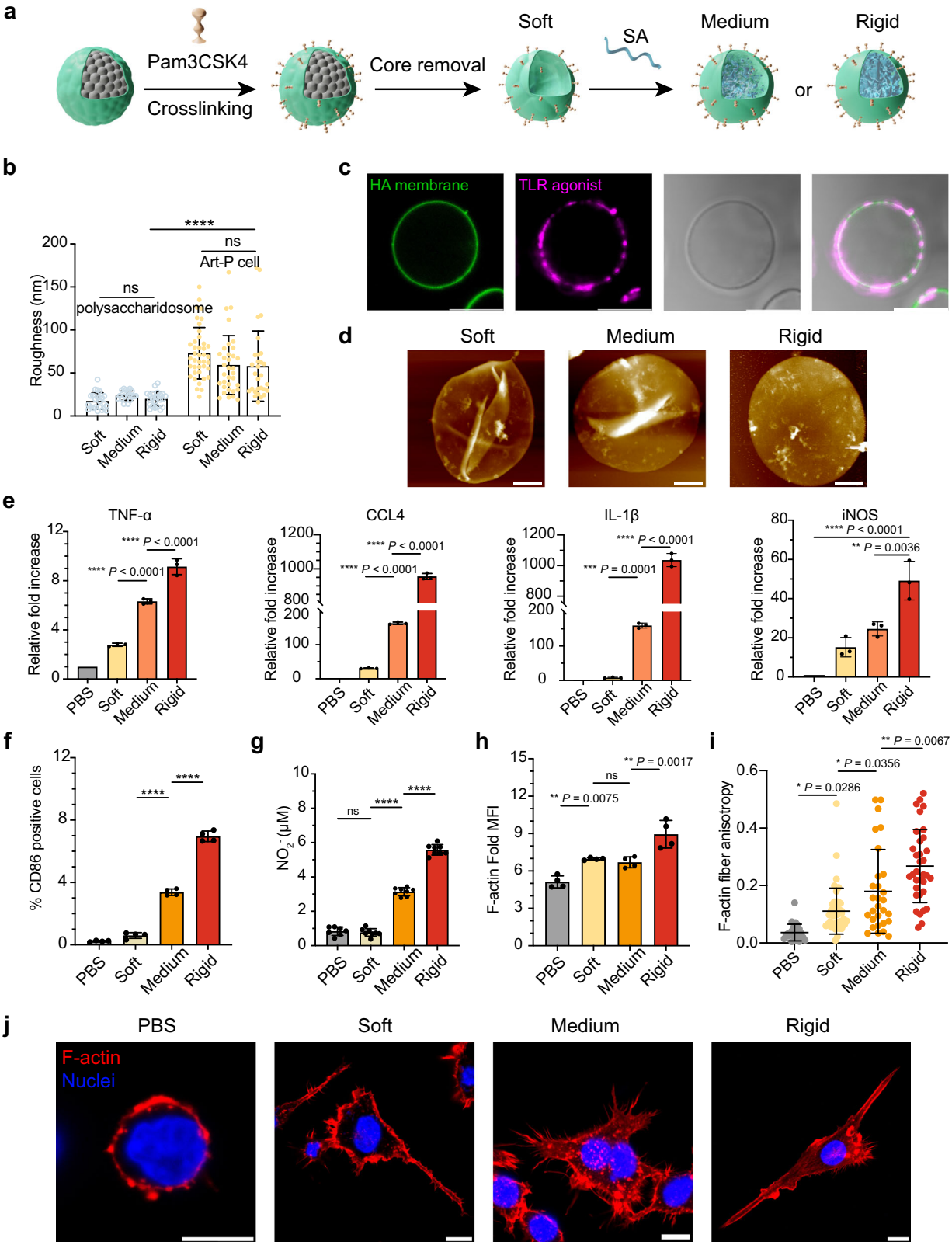

demonstrate the universality of the mechano-transduction axis involving protocell rigidity, pseudopodia, and macrophage polarization, we constructed Art-P cells with comparable structural, surface and mechanical properties and relatively reduced size (d = 6.21 ± 0.78 μm, Fig. 3f, Supplementary Fig. 16, see Methods). We also varied the pathogen-mimicking ligands employed, transitioning from the agonist for TLR1/2 to an agonist for TLR4, which is another TLR found on cell surface. Additionally, we investigated the cellular response in primary macrophages, the bone marrow-derived macrophages (BMDMs). The persistence of rigidity-induced pseudopodia and polarization was consistently observed under all conditions (Fig. 3g, i; Supplementary Fig. 17a, b) The rigidity-mediated formation of more slender pseudopodia were also quantified and validated (Fig. 3h, j). Particularly, macrophages were equipped with robust pseudopodia to catch the

Fig. 2 | Rigid Art-P cells promote the inflammatory response of macrophages and stress fiber generation. a Scheme of the process leading to Art-P cell construction. Pam3CSK4 is covalently attached to the membrane before template removal. SA is subsequently trapped inside to adjust rigidity. **b** Surface roughness plots of soft, medium, and rigid air-dried polysaccharidosomes before (blue) and after (yellow) Pam3CSK4 attachment (data are mean ± s.d. from each field (n); ≥50 artificial cells; $n = 24$ for soft, 19 for medium, and 23 for rigid polysaccharidosomes; n = 40 for soft, 34 for medium, 29 for rigid Art-P cells). ns $P > 0.05$, **** $P < 0.0001$. **c** Confocal microscopy images of Art-P cells following surface functionalization of polysaccharidosome membrane (green) with TLR agonist (Pam3CSK4, purple, labeled by 1,1′-dioctadecyl-3,3,3′,3′-tetramethylindodicarbocyanine, 4-chlorobenzenesulfonate salt (DiD)). Scale bars = 10 μm. **d** AFM images of air-dried soft, medium, and rigid Art-P cells (scale bars = 10 μm). **e** Plots showing relative fold increase of the gene expression levels of pro-inflammatory cytokines (tumor necrosis factor α, TNF-α; chemokine (C-C motif) ligands 4, CCL4; interleukin 1β, IL-1β; inducible nitric oxide synthase, iNOS) by macrophages incubated with Art-P cells relative to the control sample (PBS) as analyzed by RT-qPCR, three biological replicates. **f** Plots showing the percentage of CD86 positive macrophages (four biological replicates), **** $P < 0.0001$, and **g** NO_2^- concentration in culture medium from macrophages that are co-cultured with PBS or Art-P cells (PBS, seven biological replicates; Art-P cell groups, eight biological replicates), **** $P < 0.0001$. **h** Mean fluorescence intensity of RITC-phalloidin labeled F-actin of macrophages (four biological replicates), and **i** quantification of actin anisotropy after co-culture with PBS or Art-P cells ($n = 25$ for PBS, 44 for soft, 29 for medium, and 34 for rigid, three biological replicates). For **e**–**i**, data are mean ± s.d. **j** Confocal microscopy images of macrophage (blue) F-actin (red) morphology after co-culture with PBS or Art-P cells (scale bars = 10 μm). In **b**, **e**–**i** significance was determined by one-way ANOVA followed by Tukey's multiple comparison test. Source data are provided as a Source Data file.

smaller-sized rigid Art-P cells prior to engulfment (Fig. 3g; Supplementary Fig. 17c).

Robust pseudopodia anchor to artificial cells through HA-CD44-actin mechanosensitive molecular clutch

We next explored how the pseudopodia transmit the mechanical signal from Art-P cells to macrophages. HA, the building block of Art-P cell, is one of the key components of pathogen glycocalyx, covering the cell membrane. The HA portion acts as an adhesive bridging molecule that is involved in intercellular communication through binding with CD44[33,50]. CD44, a transmembrane adhesion receptor, is upregulated on immune cells and regulates cell-cell communication. Its cytoplasmic-tail region can be crosslinked to the actin cytoskeleton by the ERM (ezrin, radixin, and moesin) proteins[51]. To validate the hypothesis that HA-CD44 serves as the mechanoresponsive element connecting the Art-P cell and macrophage cytoskeleton, we fluorescently labeled the CD44, ERM proteins, and F-actin in macrophages co-cultured with either soft or rigid Art-P cells (Fig. 4a, Supplementary Fig. 18). We observed abundant CD44 at the adhesion interface and in the pseudopodia surrounding the rigid Art-P cell. Upon closer examination of the interface between Art-P cells and macrophages, CD44, ERM, and F-actin were recruited into close juxtaposition, especially within the slender pseudopodia at the rigid interface (Fig. 4e). Moreover, an increased rigidity led to enhanced localization of ERM proteins alongside CD44 (Fig. 4c). To validate the function of HA-CD44, we first inhibited the interaction by treating RAW macrophages with CD44 antibodies. CD44 antibodies treatment impaired the co-localization of CD44 and ERM proteins, as well as pseudopodia extension on rigid Art-P cells (Fig. 4c, Supplementary Fig. 19). Furthermore, complete blockade of CD44-HA interaction was achieved by genetic knockout (KO) of CD44 in human THP-1 macrophages. Conserved rigidity-induced co-localization of CD44 and ERM proteins was observed in both murine and human macrophage pseudopodia (Supplementary Fig. 20a). Notably, the KO of CD44 not only profoundly inhibited the signal from ERM proteins but also impaired pseudopodia formation and macrophage activation (Fig. 4d, Supplementary Fig. 20b, c). These results suggest that the HA-CD44 anchor links the cell's interior cytoskeleton to the extracellular artificial cell, facilitating force transmission and mechano-sensing.

To examine interfacial force loading, we anchored tension-responsive DNA-based tension probes (tension gauge tether, TGT) within Art-P cell membranes (Fig. 4f)[30,52]. This molecular force tool generates a fluorescent turn-on signal upon reaching its activation threshold at the piconewton (pN) level, where rupture of the DNA duplex releases pre-quenched fluorophores—a system widely validated across diverse surfaces[53–56]. We co-assembled aminated TGTs with HA-NH_2 on the surface of the sacrificial templates, crosslinking HA-NH_2 with tension probes (See Methods, Supplementary Fig. 21a). Membrane deformation triggered TGT activation (Supplementary Fig. 21b, c), enabling Art-P cells to report macrophage-exerted forces at adhesion interfaces.

Macrophages co-cultured with soft or rigid TGT-functionalized Art-P cells for 1 h and 5 h, respectively, induced increasing TGT activation signals in rigid artificial cells (Fig. 4g, h, Supplementary Fig. 22). The activation signals were pronounced in rigid Art-P cells engaged with macrophages, coinciding with enhanced peri-junctional F-actin activity, indicating amplified force generation at stiff interfaces. This rigidity-dependent force exertion was further validated using smaller Art-P cells (Supplementary Fig. 24). CD44 KO macrophages showed a reduction in tension generation, further corroborating the force loading and transmission via the HA-CD44 anchor (Fig. 4g, h, Supplementary Fig. 25).

The above findings suggest that the HA-CD44-actin linkage functions as a mechanosensitive molecular clutch, firmly anchored to the rigid artificial cell surface, thereby facilitating the force transmission, extension of robust pseudopodia and initiating downstream translation of a mechanical signal into a biochemical signal (Fig. 4i). The distinct behavior is conserved in both murine and human macrophages. Such pseudopodia exhibited by macrophages in communication with artificial cells may be attributed to variations in interface properties[14,57,58]. For example, the mechanical signals associated with the artificial cells are presented in a free-floating manner and possess a three-dimensional curved surface, which could induce strong attachment and necessitate the assembly of robust pseudopodia. Interestingly, analogous pseudopod behavior has been observed in living cell-cell interactions, for example at the immunological synapse interface formed by T cells and antigen-presenting cells[59,60], and in macrophage/bacteria interactions in microenvironments accessible within the reach of their invasive filopodia[61], suggesting that extending robust pseudopodia is a distinct behavior for sensing mechanical signals presented at the cellular level.

Actin-supported pseudopodia facilitate the response of macrophages to rigid artificial pathogen cells

The above results reveal that on contact rigid Art-P cells facilitate pro-inflammatory polarization of macrophages and enhance force generation via pseudopodia extension, which involves a mechanosensitive molecular clutch. Pseudopodia are active extensions of membranes and cytoskeletons, in which polymerization of branched actin networks generates a protrusive force that reaches beyond the normal cell boundary[62,63]. To elucidate the link between the rigidity of the Art-P cells, pseudopodia dynamics and polarization, as well as how the rigid Art-P cells enhance the strength of the pseudopodia, we used F-actin staining to determine the interfacial ultrastructure. The data indicated that the actomyosin cytoskeleton was condensed inside the macrophage pseudopodia formed at the adhesion interface (Fig. 5a). Remarkably, thin and independent bundles of actin filaments were observed at the rigid interface, anchoring into the membrane in a

https://doi.org/10.1038/s41467-025-63581-1

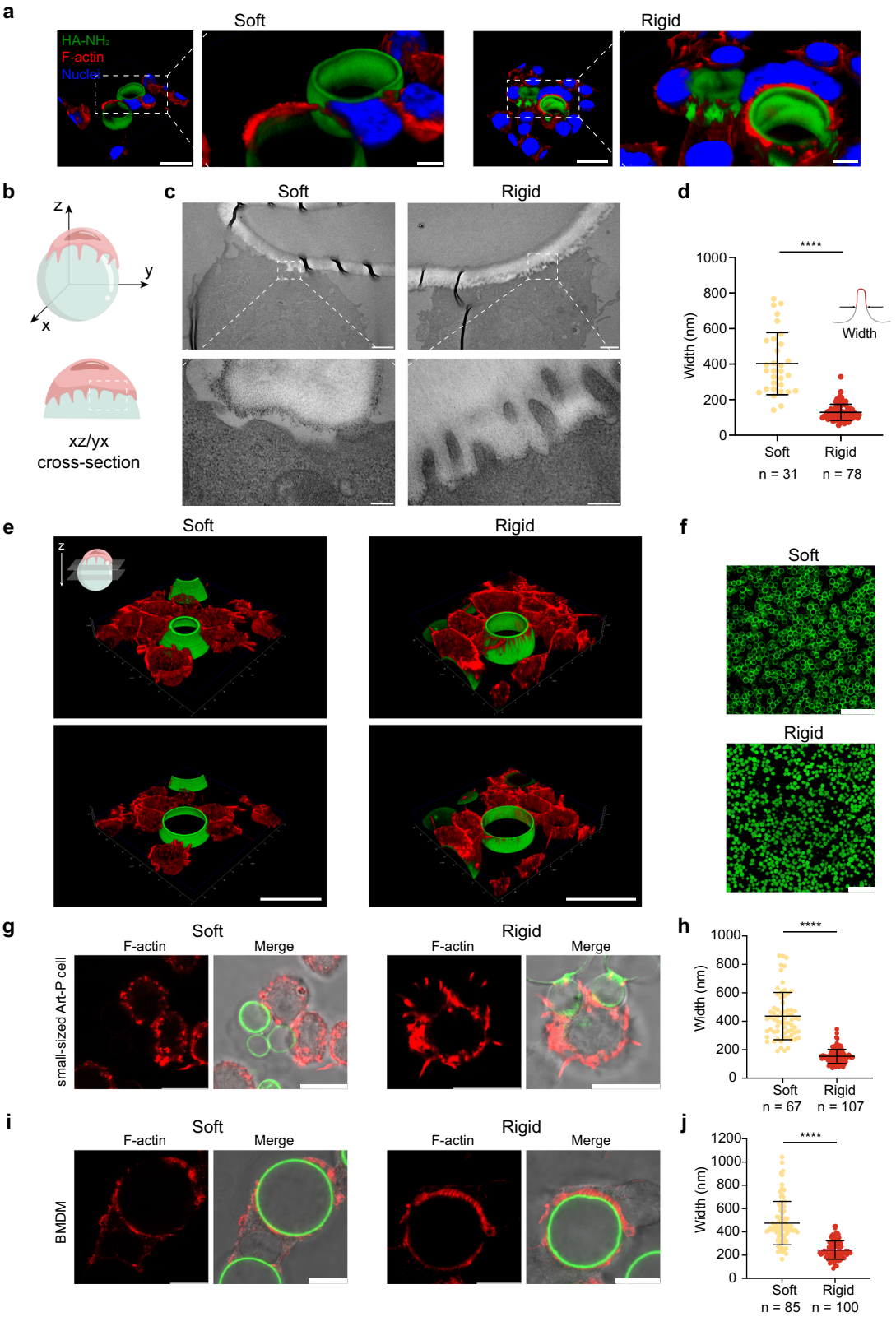

perpendicular manner with respect to the adhesion surface, thereby resulting in a clear deformation of the rigid Art-P cell surface.

Recent evidence indicates that due to the lack of compliance, rigid surfaces result in rapid force loading rates of adhesion bonds that connect the microenvironment and cell cytoskeleton[5,64,65]. The force is loaded faster than the lifetime of the cell adhesion bonds, thus resulting in the maturation of adhesion complexes and actin-based reinforcement. Given these considerations, we suggest that the rigid Art-P cells induce extensive actin polymerization by increasing the force loading rate. In such a mechanism, the enhanced actomyosin cytoskeleton tension drives active membrane protrusion and pseudopodia extension so that they can be inserted deeply into the Art-P cell membrane. Previous studies have demonstrated that pseudopodia dynamics govern immune cell polarization through intense membrane

Fig. 3 | Macrophages extend robust pseudopodia to anchor onto rigid artificial pathogen cells. a 3D reconstructed confocal microscopy images of macrophages that surround soft (left) or rigid (right) Art-P cells (green, FITC labeled HA membrane of Art-P cell; red, RITC-phalloidin labeled F-actin; blue, DAPI-labeled macrophage nucleus). Scale bars = 25 μm (enlarged, 5 μm). **b** Graphics depicting the confocal scanning planes shown in (**c**). **c** Representative TEM micrographs showing macrophage pseudopodia extending at the contact junctions with soft or rigid Art-P cells; scale bars = 1 μm (top); = 200 nm (bottom). **d** Graphic showing the width of macrophage pseudopodia on soft versus rigid interfaces, as characterized by TEM micrographs (data are mean ± s.d., soft, $n = 31$; rigid, $n = 78$), **** $P < 0.0001$. **e** The 3D reconstructed confocal microscopy images of macrophage pseudopodia that facilitate mechano-sensing (inserted graphics showing the direction of clipping). Scale bars = 25 μm. **f** Confocal microscopy images of small-sized soft (top) and rigid (bottom) Art-P cells (d = 6.21 ± 0.78 μm, mean ± s.d.). Scale bars = 50 μm. **g** Confocal microscopy images demonstrate that macrophages (RAW 264.7) utilize similar pseudopodia to sense the mechanical signal presented by small Art-P cells, while **i**, BMDMs also employ them to sense the mechanical signal presented by large Art-P cells functionalized by TLR4 agonist. Scale bars = 10 μm. Graphic showing the width of macrophage pseudopodia (**h**) in g (data are mean ± s.d., $n = 67$ for the soft group, $n = 107$ cells for the rigid group), **** $P < 0.0001$, and (**j**) in i (data are mean ± s.d., $n = 85$ for the soft group, $n = 100$ for the rigid group), as characterized by high-resolution confocal micrographs, **** $P < 0.0001$. In **d**, **h**, **j**, significance was determined by a two-tailed, unpaired *t*test. Source data are provided as a Source Data file.

deformation and subsequent alterations in membrane mechanical microenvironments[66–68]. To investigate this further, we used the mechanosensitive Flipper-TR probe, which responds to tension in cells[69], and disrupted force generation using low-dose latrunculin-A (Lat-A, 100 nM) to inhibit cytoskeleton tension[24,70]. Fluorescence lifetime imaging microscopy (FLIM) of macrophages at rigid Art-P cell interfaces revealed an increase in fluorescence lifetime (τ), visualized as a blue-to-green-to-red shift in pixel colors. This result indicated elevated tension in the cellular membrane and suggested significant alterations in membrane mechanical microenvironments (Fig. 5b, c). CD44 KO macrophages showed reduced membrane tension, further corroborating HA-CD44-mediated force loading and transmission (Supplementary Fig. 23). Representative TEM and confocal images further confirmed that Lat-A efficiently weakened pseudopodia at rigid interfaces, without entirely inhibiting F-actin polymerization, resulting in a diminished ability to firmly catch the Art-P cells (Fig. 5a, d). Critically, Lat-A treatment disrupted HA-CD44-actin clutch docking (Fig. 5f-h). Membrane CD44 maintained its ability to recruit ERM proteins at the interface but failed to generate robust pseudopodia for catching and sensing rigid Art-P cells without support from F-actin-generated force (Fig. 5f, h). Hence, force generated through actin polymerization is essential both for pseudopodia maintenance and mechano-sensing (Fig. 5e). To investigate the relationship between actin dynamic and polarization, we analyzed the typical pro-inflammatory markers of macrophages, revealing that treatment with Lat-A also attenuated the acquisition of a pro-inflammatory phenotype in macrophages co-cultured with either soft or rigid Art-P cells (Fig. 5i–k, Supplementary Fig. 26). The inhibition of pseudopodia and pro-inflammatory response was also observed in conditions involving smaller size of Art-P cells, stimulation with TLR4 agonist, and primary macrophages BMDMs (Supplementary Figs. 17, 27).

Macrophage pseudopodia exhibit remarkable plasticity in morphological changes, with subtle differences that may play a critical role in distinct cellular processes. Various surface opsonized ligands, such as complement molecules[28], IgG[71], and phosphatidylserine[72], have been reported to trigger the formation of different membrane protrusions, including flattened membrane ruffles, broad lamellipodia, and finger-like filopodia. These structures facilitate macrophage-mediated target examination and discrimination through intrinsic force-dependent mechanisms[68]. Furthermore, the above results demonstrate that force generation and pseudopodia-mediated adhesion were also essential for probing mechanical signals presented at the cellular level and initiating the inflammatory response. Advanced techniques specifically designed to modulate localized force generation are required for a more in-depth investigation. It has also been reported that enhanced actin polymerization produces an increase in cellular elasticity[39,73,74]. However, the mechanical coupling between the microenvironment and cellular mechanical properties associated specifically with the cellular detection of rigidity and modulation of immune response remains essentially unknown. Our results suggest that mechano-transduction has a key role in these processes.

Mechanosensitive ion channel Piezo1 and RhoA/ROCK signaling are involved in pseudopodia-mediated inflammatory response

Given that the phenotype and function of cells are regulated by gene transcription, we proceeded to investigate how the mechanical tension induced by interaction of the macrophages with rigid Art-P cells is transduced into biochemical signals. The application of force can directly activate mechanosensitive effectors such as ion channels, receptors, and transcriptional factors[75]. Alternatively, it modulates the details of protein-protein interactions, resulting in downstream alterations in signaling cascades. Specifically, we investigated Piezo1 and RhoA/ROCK signaling as representative examples of the above-mentioned two mechano-activation strategies.

Piezo1, which has been recently identified as a mechanically activated ion channel with high affinity for calcium, is closely involved in regulating the inflammatory response[76,77]. As increased membrane tension was observed during the extension of macrophage pseudopodia, we speculated that the increased membrane tension resulting from pseudopodia extension could activate the Piezo1. Firstly, we observed the upregulation of Piezo1 in macrophages cultured with more rigid Art-P cells at both gene and protein levels (Fig. 6a, Supplementary Figs. 28a, 31a). Upon mechanical activation, Piezo1 functions as an ion channel and promotes the influx of calcium ions (Ca^{2+})[25,39]. We assessed the cytosolic Ca^{2+} level as a functional indicator of Piezo1 activity. The rigidity-dependent increase in cytosolic Ca^{2+} was observed by staining cells with Fluo-4 AM (Fig. 6c-d, Supplementary Fig. 28b). To assess the role of Piezo1, we utilized a Piezo1 KO line of RAW macrophage or treated normal RAW with Yoda1 to either inhibit or activate Piezo1 function. Upon loss of Piezo1, bursts of actin-filled pseudopodia extension were blocked, and the inflammatory response was impaired (Fig. 6b, Supplementary Fig. 29). Treatment of macrophages with the Piezo1 agonist Yoda1 further augmented the activation of Piezo1 induced by artificial cell rigidity, leading to increased pseudopodia formation and Ca^{2+} influx (Fig. 6a, c, d, Supplementary Figs. 29, 30). Yoda1 operated dose-dependently, equalizing Ca^{2+} responses between soft and rigid Art-P cells. (Supplementary Figs. 31, 32). Conversely, treatment with Lat-A resulted in contrasting responses, erasing the increased levels of Piezo1 expression and cytosolic Ca^{2+} level. The obtained results confirm the involvement of Piezo1 in the mechano-transduction at the interface between artificial and living cells. Together, macrophages exhibit enhanced intracellular forces on rigid Art-P cells, changing membrane tension and the mechanical microenvironment, which activates Piezo1. Consequently, this facilitates mechano-sensing and calcium enrichment, which have been prominently associated with macrophage pro-inflammatory response[25,39].

As a crucial mechanosensitive pathway, RhoA/ROCK signaling shows a close connection with both actin reorganization and polarization of macrophages[78,79]. We therefore considered whether RhoA/ROCK signaling was relevant to this protocell rigidity-pseudopodia-inflammatory response functional axis. In response to increased rigidity of the Art-P cells, the gene expression of representative molecules of the small GTPases families, Cdc42 and RhoA, exhibited a

https://doi.org/10.1038/s41467-025-63581-1

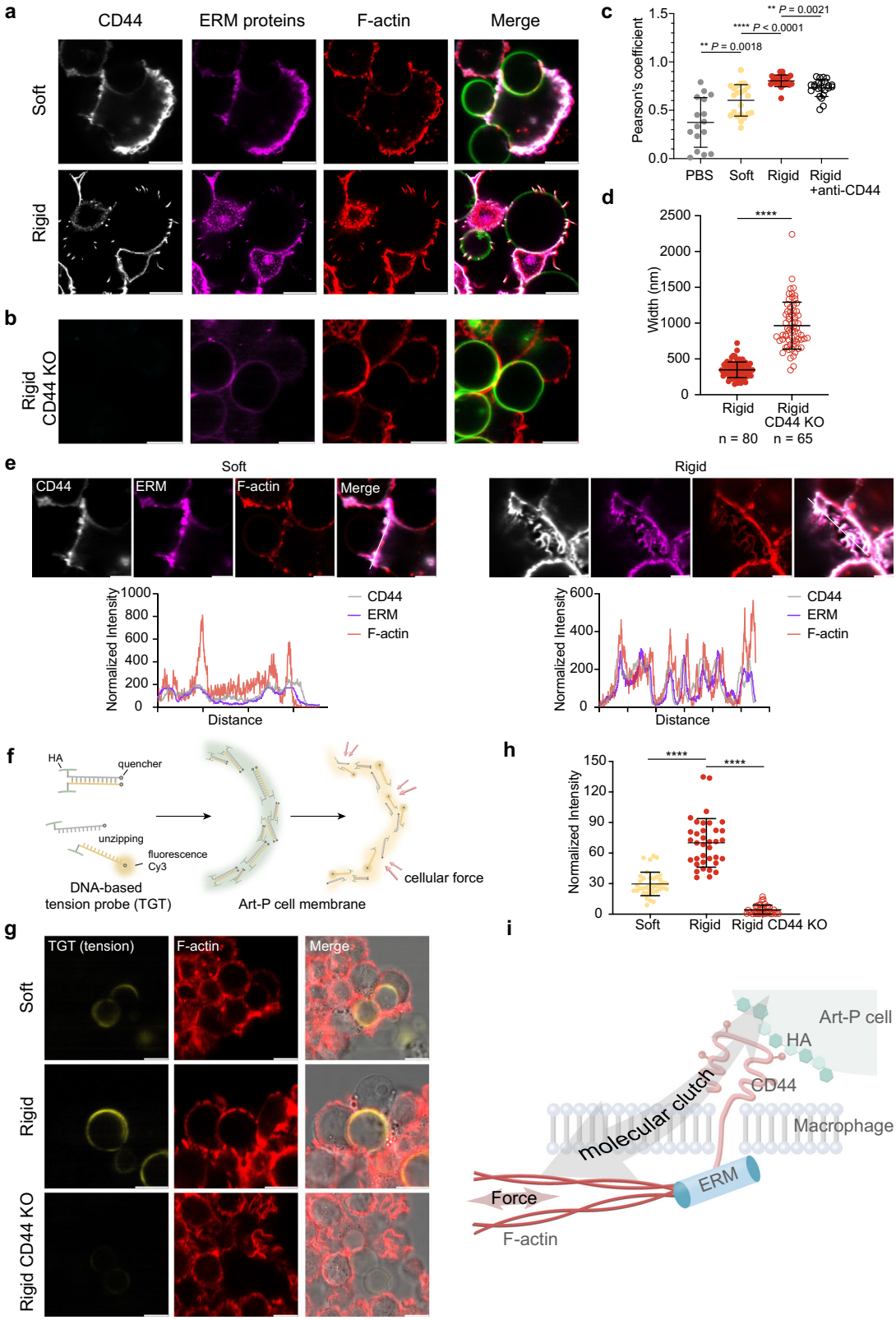

trend towards upregulation (Supplementary Fig. 33). Through immunofluorescence analysis, we confirmed the significant increase in RhoA expression, which implies its functional involvement (Fig. 6e; Supplementary Fig. 34). To further validate the activation of RhoA, we quantified the GTP-bound active form of RhoA using the G-LISA assay (Fig. 6f)[78]. Additionally, we employed the ROCK inhibitor Y27632 to investigate the involvement of RhoA/ROCK signaling. The level of the active form of RhoA was elevated in rigid Art-P cells, whereas treatment with either Y27632 or Lat-A inhibited RhoA activation. The impairment of RhoA activation was further confirmed in CD44 KO THP-1 macrophages, providing additional evidence for the involvement of the CD44-HA in mechanotransduction (Supplementary Fig. 35). Correspondingly, Y27632 treatment impaired pseudopodia formation, while both inhibitors effectively suppressed

Fig. 4 | Mechanosensitive clutch anchors the pseudopodia to the artificial cells and facilitates mechano-transduction. Confocal microscopy images of F-actin, CD44, and ERM proteins in (**a**) RAW macrophages after 24 h of co-culturing with soft, rigid Art-P cells, or (**b**) rigid Art-P cells with CD44 KO THP-1 macrophages; scale bars = 10 μm. **c** Pearson's correlation coefficient values for colocalization of CD44 and ERM proteins in RAW macrophages. The average Pearson's correlation coefficients were calculated from randomly selected cells that interact with Art-P cells in each group (data are mean ± s.d. from each field (n), $n = 16$ for PBS, 22 for soft, 23 for medium, 23 for rigid, cells ≥50; three biological replicates). **d** Graphic showing the width of THP-1 macrophage pseudopodia on rigid interfaces, comparing normal versus CD44 KO macrophages, as characterized by high-resolution confocal micrographs (data are mean ± s.d., normal, $n = 80$; KO group, $n = 65$), **** $P < 0.0001$. **e** Confocal microscopy images demonstrate the recruitment of CD44, ERM proteins, and F-actin into close juxtaposition at the Art-P cell/macrophage interface, and (below) the normalized fluorescence intensity of CD44 (gray), F-actin (red) and ERM proteins (purple) corresponding to images. Scale bars = 5 μm. **f** Scheme illustrating the functionalization of DNA-based tension probes within the Art-P cell membrane for reporting macrophage force exertion at the artificial-living cell interface. **g** Confocal microscopy images of activated DNA-based tension probes (yellow) and F-actin (red) in THP-1 macrophages after 5 h of co-culture (scale bars = 10 μm), and **h**, the corresponding quantification of normalized fluorescence intensity of tension probes (soft, $n = 38$; rigid, 36; KO group, 35; data are mean ± s.d., **** $P < 0.0001$). **i** The graphical presentation of the HA-CD44-actin linkage serves as a mechanosensitive molecular clutch, facilitating the mechanotransduction in macrophage pseudopodia. In **c**, **d**, significance was determined by a two-tailed, unpaired *t*test; **h**, significance was determined by one-way ANOVA followed by Tukey's multiple comparison test. Source data are provided as a Source Data file.

the pro-inflammatory response in macrophages (Fig. 6e, f; Supplementary Fig. 36a). These results suggest that RhoA/ROCK signaling pathway facilitates the mechano-transduction axis from artificial cells to macrophages. Our findings regarding the Piezo1 and RhoA/ROCK signaling further corroborate that cellular responses to cell-exerted forces involve a feedback loop of inside-outside-in that couples to the mechanical properties of the extracellular microenvironment[80].

Both intracellular Ca^{2+} enrichment and RhoA/ROCK signaling have been reported to upregulate nuclear factor kappa-light-chain-enhancer of activated B cells (NF-κB) activation[27,81], which is an essential transcription factor that promotes inflammation[82]. We found that macrophages cultured with rigid Art-P cells exhibited enhanced NF-κB activation, as indicated by the nuclear translocation degree of NF-κB heterodimers (Fig. 6g, h, Supplementary Fig. 36b). While disturbing Piezo1, RhoA/ROCK signaling, or actin polymerization all led to affected NF-κB activation.

Overall, Piezo1, functioning as a mechanosensitive ion channel, sensed mechanical signals from Art-P cells, regulated Ca^{2+} influx, and participated in the pseudopodia-mediated inflammatory response. Additionally, we observe a robust correlation between RhoA/ROCK signaling and this mechano-transduction axis between Art-P cells and macrophages. These results suggest the possibility of crosstalk between the two mechanically activated strategies (Fig. 6i). Specifically, the pathways translate mechanical forces into intracellular biochemical events and activate NF-κB bound to specific gene promoters. This event could potentially serve as a hallmark mechanism[25], thereby modulating the expression of pro-inflammatory proteins in macrophages adhered to the Art-P cells.

Discussion

As a critical member of the immune cells with active migratory capacity, macrophages can scan and sense signals from other cell surfaces to regulate physiological and pathological processes, and accordingly, their phenotypes are strongly regulated by physical cues[42]. To gain a comprehensive understanding of the mechano-crosstalk between living and artificial cells, here we construct model Art-P cells with living pathogen-inspired properties. We fine-tune the rigidity of Art-P cells to achieve a comparable level with that of living cells and use this new platform to decouple cell-presented mechanical signals. Our investigation shows that macrophages extend actin-mediated robust pseudopodia on their adhesion interface with rigid Art-P cells, employing a mechano-sensitive HA-CD44-actin molecular clutch to facilitate stable adhesion and signal probing. This mechanism serves as an essential way to enhance the mechano-transduction and pro-inflammatory response. We further reveal that the membrane ion channel Piezo1, RhoA/ROCK signaling and downstream NF-kB activation are involved in translating the mechanical signals into biochemical interactions, representing two prototypical mechano-transduction strategies (Fig. 7). Although the precise molecular mechanism may vary in the context of phagocytosis of smaller Art-P cells, it is evident that the protocell rigidity-pseudopodia-inflammatory response functional axis remains persistent. The distinct pseudopodia extended by the macrophages are similar in morphology and function to the attachable structures of macrophages and lymphocytes in immunological synapses, thereby suggesting that this may be a unique behavior used by macrophages to sense signals presented at the cellular level.

Art-P cells serve as physiologically relevant platforms that replicate cell-mimicking contexts, offering a promising tool for studying membrane signal-mediated intercellular interactions—particularly the deciphering of mechano-crosstalk. The ability to independently functionalize both the membrane and the endoplasm allows for a more precise understanding of the complex mechanisms underlying intercellular communication. Consistent with previous studies[37,83], our results demonstrate that an important relationship exists between cell morphology and macrophage polarization. However, contradictory results and conclusions have been reached through comparisons of the polarization in response to mechanical cues presented by either ECM-mimicking substrates or particle-based models[84,85]. For example, Kang et al. observed that macrophages with suppressed F-actin assembly tended to acquire pro-inflammatory polarization on a magnetic nano-helix deposited material surface[26]. Liu et al. proposed that actin polymerization and myosin-dependent cytoskeletal contractility were enhanced via pro-healing activation to a greater extent in comparison with pro-inflammatory activation when the macrophages were cultured on micropatterned substrates[68]. Such conflicting observations may result from the different interfacial properties. In particular, the surface of ECM-mimicking materials is a relatively fixed two-dimensional planar structure, with pro-inflammatory signals being dissolved in the surrounding medium. The synthesis of suitable microparticles can be quite intricate, and it typically lacks the compartmentalization architecture characteristic of living cells[28,72]. In contrast, template-directed membrane self-assembly and surface functionalization enable the efficient construction of uniform and customizable artificial cells. The resulting Art-P cells have a cell-mimicking, free-floating, and three-dimensional curved microcompartment. Consequently, macrophages must adhere firmly so that they can probe the surface-presented inflammatory signals. This discrepancy highlights the dramatic impact of the signal presentation microenvironment and the significance of our current work.

Further advances in the design of artificial cells should enable increased regulation of the surface and mechanical properties such that a universal platform for studying mechanical signal communication between cells could be implemented. Intracellular responsiveness within artificial cells could also be investigated to gain insight into natural-artificial bi-directional interactions and thereby narrow the gap between fundamental research and potential bioengineering applications. In addition, our findings indicate that macrophages have rigidity

https://doi.org/10.1038/s41467-025-63581-1

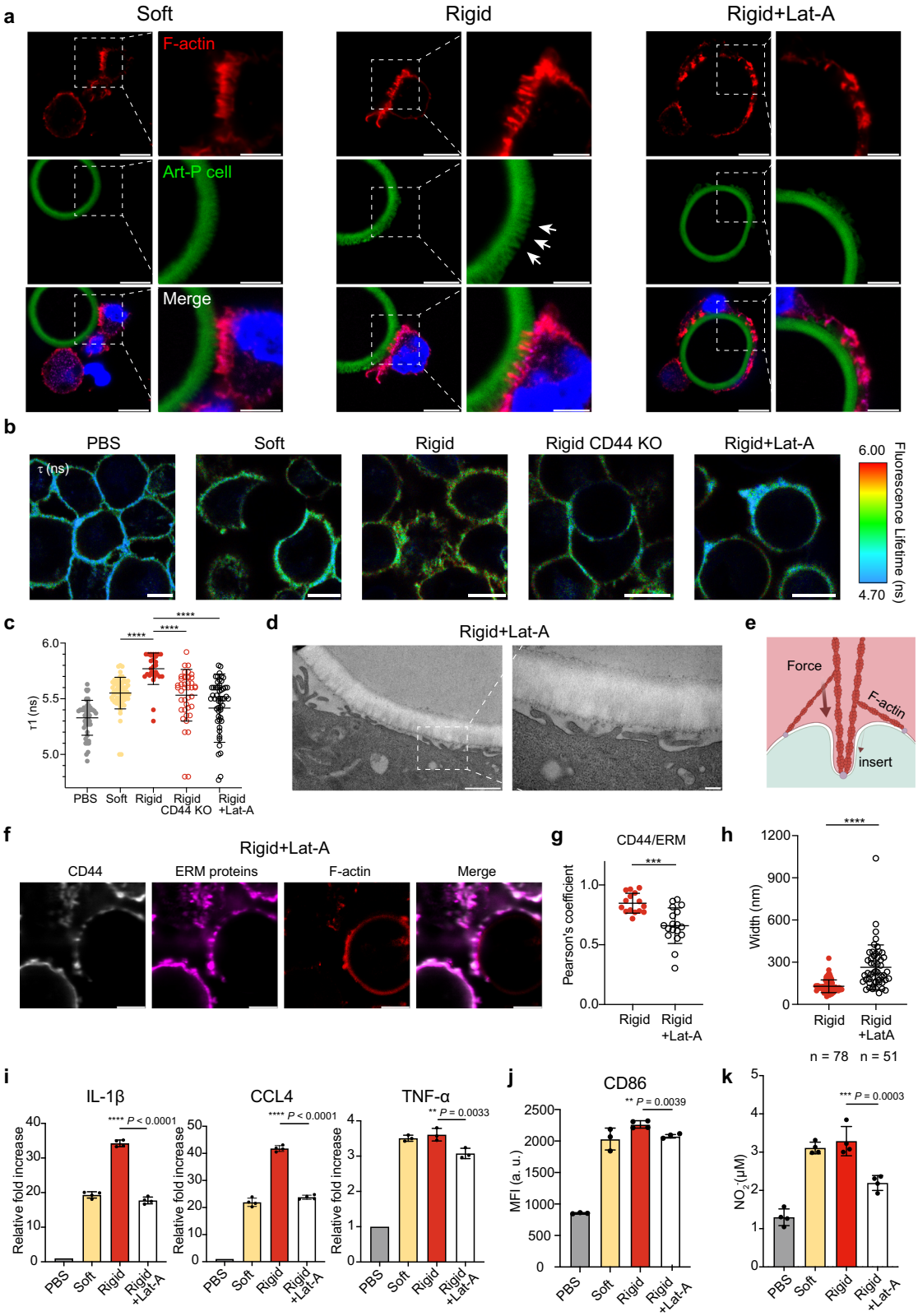

sensors that act at different length scales, with dimensions ranging from the nanometer to the micrometer scales. This will provide more opportunities for the bottom-up construction of artificial cells with multi-scale biomimetic structures that can chemo-mechanically communicate with live cells.

Finally, a better understanding of how cell-presented mechanical signals regulate specific disease-associated macrophage functions could have a vital role in enabling the development of immune-targeted therapies for disease treatment. For instance, tumor cells exhibit a low elastic modulus, high mobility, and can evade immune surveillance via multiple strategies[86–88]. Our findings suggest a new perspective regarding the mechanisms involved in this process, in which targeting cell-cell interactions in combination with conventional therapies has the potential to improve therapeutic outcomes.

Fig. 5 | Actin polymerization has an essential role in supporting macrophage pseudopodia extension and inflammatory response. a Confocal microscopy images of macrophage interactions with Art-P cells showing extension of robust pseudopodia and insertion into the Art-P cell membrane (arrows: deformation of Art-P cell membrane; green: Art-P cell membrane, red: F-actin, blue: nucleus). Scale bars = 10 μm, =5 μm (magnified). **b** Images showing the change in fluorescence lifetime (τ) of Flipper-TR probe in THP-1 macrophages. Scale bars = 10 μm. **c** Graphic showing individual τ values in selected regions of interest (ROIs) across interfaces (data are mean ± s.d., $n = 49$ for PBS, 62 for soft, 30 for rigid, 42 for CD44 KO, and 55 for Lat-A group, three biological replicates, $^{****}P < 0.0001$). **d** TEM micrographs showing macrophage pseudopodia extending at the rigid contact junctions are weakened by Lat-A treatment; scale bars = 1 μm (left); = 200 nm (right). **e** Graphic of the actin-mediated insertion of macrophage pseudopodia into artificial cell membrane. **f** Confocal microscopy images showing macrophage interactions with rigid Art-P cells following Lat-A treatment. Scale bars = 10 μm. **g** Pearson's correlation coefficient values for colocalization of CD44 and ERM proteins in macrophages (data are mean ± s.d. from each field (n); rigid, $n = 15$; Lat-A, 18, three biological replicates; cells ≥50. $^{***}P = 0.0001$). **h** Graphic showing the width of macrophage pseudopodia on rigid interfaces (normal, $n = 78$; Lat-A, 51), as characterized by high-resolution confocal micrographs. Data are mean ± s.d., $^{****}P < 0.0001$. **i** Plots showing relative increase in pro-inflammatory cytokine gene expression in macrophages relative to the control (PBS), as analyzed by RT-qPCR (data are mean ± s.d., three biological replicates). Plots showing the percentage of CD86 positive macrophages (**j**) and NO_2^- concentration (**k**) in macrophage culture medium (data are mean ± s.d., three biological replicates). In **g**, **h**, **j** significance was determined by a two-tailed, unpaired *t*test; **c**, **i**, **k** significance was determined by one-way ANOVA followed by Tukey's multiple comparison test. Source data are provided as a Source Data file.

Methods

Characterization

^{1}H NMR spectra were recorded using an Avance III 600 MHz spectrometer (Bruker, Switzerland) in D_2O (δ = 4.79). Optical and fluorescence microscopy characterization was performed with an Axio Scope.A1 upright fluorescence microscope at 20×, 50×, and 100× magnifications. Images were analyzed using AxioVision and ImageJ software. Confocal microscopy images were captured with a Leica TCS SP8 STED 3X Super-Resolution Multiphoton Confocal Microscope using the Adaptive Focus Control mode to correct focus drift during time-lapse capture. The microscope was equipped with the following lasers: a 65 mW Ar (458, 488 nm lines), a 20 mW solid-state yellow (561 nm), a 10 mW Red He/Ne (633 nm), and a 50 mW UV 405 nm diode. All measurements were performed in an environmental chamber that was maintained at 25 °C. Images were analyzed using Las X confocal microscopy software version V3.1.1. Transmission electron microscopy (TEM) images were recorded using a FEI Tecnai G2 Spirit BioTwin transmission electron microscope (120 kV, FEI, U.S.A.). The zeta potentials of polysaccharide derivatives were measured using a ZETASIZER Nano series instrument (Malvern Instruments, UK) at 25 °C. Flow cytometry/fluorescence-activated cell sorting (FACS) measurements were performed with a BD LSRFortessa system that was equipped with 488, 561, and 633 nm lasers and operated at low pressure with a 100 μm sorting nozzle. 2D dot plots of the forward-scattered (FSC) and side-scattered (SSC) light were determined for a total of >10,000 particles, and histograms of the number of counts against corresponding fluorescence intensity (e.g., tetramethylrhodamine (TRITC) or allophycocyanin (APC)) were determined. Data analysis was performed with FlowJo 10.3 software.

Construction of polysaccharidosomes with tunable rigidity

Polysaccharidosomes were prepared by single electrostatically-directed assembly on sacrificial micro-templates.

To synthesize the negatively charged templates, Na_2CO_3 solution (Amethyst, 99.8%, 2 mL of 0.5 M aqueous solution), $CaCl_2$ solution (Sinopharm Chemical Reagent Co., Ltd, 2 mL of 1 M aqueous solution), Dex-COOH solution (1 mL of 20 mg/mL aqueous solution), and tannic acid solution (Macklin, 1 mL of 1 mg/mL aqueous solution) were mixed together. After stirring for 40 s at 800 rpm and at room temperature, the formed particles were aged for another 3 h without any disturbance. The templates were collected by centrifugation at 120 × g for 3 min and were washed with H_2O three times.

The diameter of sacrificial micro-templates can be modulated through temperature control. To synthesize templates with a smaller diameter (in this study, d = 6.21 ± 0.78 μm), temperature was lowered to 4 °C during the stirring of Na_2CO_3 solution, $CaCl_2$ solution, Dex-COOH solution, and tannic acid solution. The formed particles were aged for another 15 min without any disturbance. The templates were collected by centrifugation at 150 × *g* for 3 min and were washed with H_2O three times.

The as-prepared templates were dispersed into 3 mL of HA-NH_2 solution (2 mg/mL), at pH 6.5 buffered by 10 mM 4-(2-hydroxyethyl)-1-piperazineethanesulfonic acid (HEPES). After 1 h of agitation, the HA-NH_2-coated templates were collected via centrifugation (120 × *g*, 3 min), washed with HEPES (10 mM, pH 6.5) twice to remove the residual HA-NH_2, and resuspended in 5 mL of PEG-bis(*N*-succinimidyl succinate) solution (Sigma, M_w = 2000 g/mol, 98%, 2 mg/mL, at pH 6.5 buffered by 10 mM HEPES). After another 4 h of agitation, the templates were collected via centrifugation. The hollow polysaccharidosomes were obtained by incubating the templates into 0.2 M EDTA solution (15 mL, at pH 8.5) for 30 min to remove the sacrificial templates. The polysaccharidosomes were collected via centrifugation (200 ×g, 3 min), and washed with H_2O three times.

The as-prepared hollow polysaccharidosomes were resuspended in 5 mg/mL (for medium) or 15 mg/mL (for rigid) sodium alginate solution (Aladdin, S00126, dissolved in 30 wt% urea solution). After another 3 h of incubation, the gel-filled medium or rigid polysaccharidosomes were collected by centrifugation, and then washed with H_2O twice. The polysaccharidosomes with different rigidity were resuspended in H_2O or the desired solvent for different testament and applications.

Construction of artificial pathogen cell

The as-prepared HA-NH_2 coated templates were modified by toll-like receptor 1/2 agonist Pam3CSK4 (N-palmitoyl-S-[2,3-bis(palmitoyloxy)-(2RS)-propyl]-[R]-cysteinyl-[S]-seryl-[S]-lysyl-[S]-lysyl-[S]-lysyl-[S]-lysine, InvivoGen) before being incubated with EDTA. Briefly, the templates were suspended in 4 mL of *N*-(3-(dimethylamino)propyl)-*N*′-ethyl carbodiimide hydrochloride (EDAC; Shanghai J & K Chemical Technology Co., Ltd.; 0.5 mg/mL) and *N*-hydroxysuccinimide (NHS, Alfa, 0.5 mg/mL) solution and activated by stirring for 10 min at room temperature. Pam3CSK4 solution (10 μL, 1 mg/mL dissolved in H_2O) was added to each batch of templates. After another 12 h of stirring at 4 °C, the Pam3CSK4-modified templates were collected and incubated with EDTA.

Alternatively, the as-prepared HA-NH_2 coated templates were modified by toll-like receptor 4 agonist lipopolysaccharide before being incubated with EDTA. Briefly, the templates were suspended in 5 mL of biotinyl-N-hydroxy-succinimide (biotin-NHS, MedChemExpress, 100 μg/mL) solution. After 3 h of stirring at room temperature, the templates were collected and washed with H_2O. Subsequently, a solution of streptavidin (5 mL, 0.1 mg/mL, Yeasen) was added to each batch of templates and allowed to react for 30 min. This was followed by the addition of biotinylated lipopolysaccharide solution (20 μL, 1 mg/mL, InvivoGen) into the mixture for an additional hour at room

https://doi.org/10.1038/s41467-025-63581-1

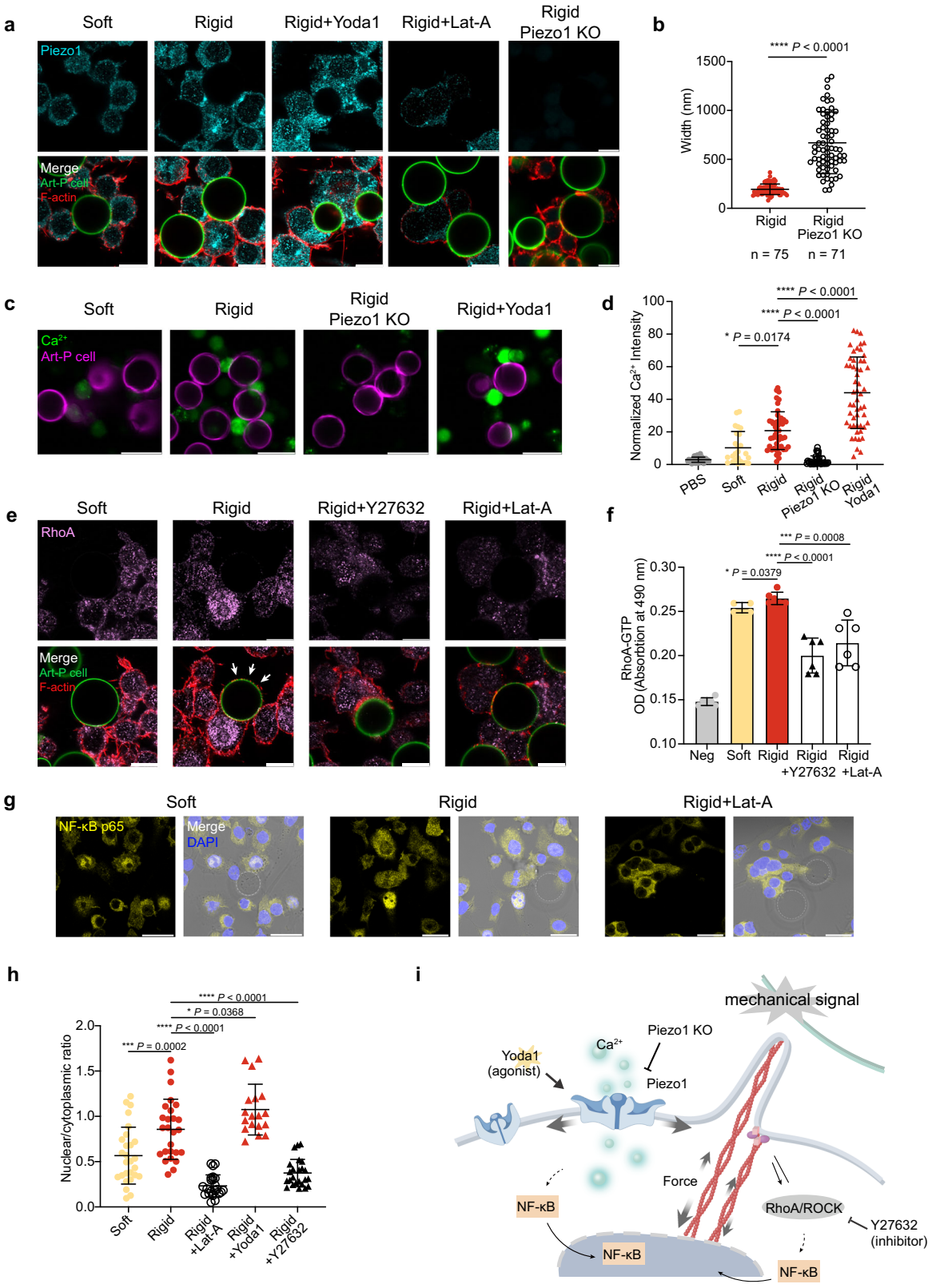

temperature. The lipopolysaccharide-modified templates were collected and incubated with EDTA.

In addition, the rigidity of the Art-P cells was tuned by the same method as was employed for the polysaccharidosomes. The sizes of the polysaccharidosomes and artificial pathogen cells were determined by optical microscope and measured by Image J software. At least thirty polysaccharidosomes or artificial pathogen cells were measured for each sample to calculate the average size and size distribution.

Construction of DNA-based tension probe functionalized Art-P cells

To investigate interfacial forces between artificial cells and macrophages, we functionalized Art-P cell membranes with DNA-based

Fig. 6 | Piezo1 and RhoA/ROCK signaling are involved in mechano-transduction. a Immunofluorescence images showing Piezo1 (cyan) and F-actin (red) localization in macrophages cultured under various conditions: with soft Art-P cells, rigid Art-P cells, rigid Art-P cells with Yoda1 (5 μM) or Lat-A treatment, or in Piezo1 KO macrophages with rigid Art-P cells (green: Art-P cells). Scale bars = 10 μm. **b** Graphic showing the width of macrophage pseudopodia on rigid interfaces, comparing normal ($n = 75$) with Piezo1 KO ($n = 71$) macrophages, as characterized by high-resolution confocal micrographs. Data are mean ± s.d. **c** Confocal microscopy images of intracellular Ca^{2+} imaging (green, Fluo-4 AM) after co-culturing with the soft or rigid Art-P cells, rigid Art-P cells with Yoda1 treatment (5 μM), or Piezo1 KO macrophages cultured with rigid Art-P cells (purple: Art-P cells). Scale bars = 25 μm. **d** Plots of the corresponding quantification of intracellular Ca^{2+} influx (data are mean ± s.d., $n = 31$ for PBS, 25 for soft, 46 for rigid, 34 for Piezo1 KO, 53 for Yoda1 group, three biological replicates). **e** Immunofluorescence images of RhoA (magenta) and F-actin (red) in macrophages (white arrows: macrophage pseudopodia); scale bars = 10 μm. **f** Plots showing RhoA activation quantified using the G-LISA assay of macrophages (data are mean ± s.d., four biological replicates). **g** Confocal microscopy images of NF-κB p65 (yellow) staining of macrophages after co-culturing with the soft, rigid Art-P cells or rigid ones with Lat-A treatment (white dashed circles: Art-P cell; scale bars = 25 μm). **h** Plots showing the corresponding quantification of nuclear/cytoplasmic p65 ratio, compared with the control group (data are mean ± s.d., $n = 25$ for PBS, 27 for soft, 26 for rigid, 23 for Lat-A treatment, 18 for Yoda1 treatment, and 24 for Y27632 treatment, three biological replicates). **i** Schematic depiction of the involvement of mechanosensitive ion channel Piezo1 and RhoA/ROCK signaling in pseudopodia-mediated inflammatory response. In **b**, **f** significance was determined by a two-tailed, unpaired *t*test; **d**, **h** significance was determined by one-way ANOVA followed by Tukey's multiple comparison test. Source data are provided as a Source Data file.

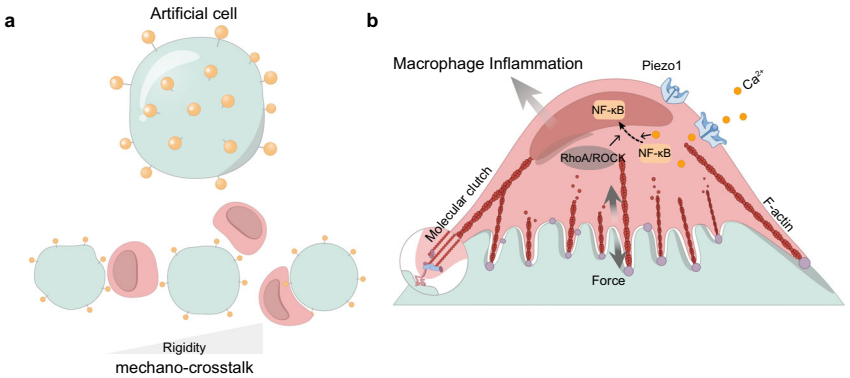

Fig. 7 | Schematic illustration depicting the mechano-crosstalk between artificial cells and macrophages. a Schematic illustration of the experimental paradigm for probing mechanical crosstalk between living cells and artificial cells. **b** Multiscale mechano-sensing apparatus of macrophages, depicting rigidity sensors operating across nanometric to micrometric dimensions.

tension probes (tension gauge tether, TGT, unfolding force = 12 pN), developed by Salaita et al.[30,54,55]. Force-triggered membrane deformation activates TGTs when tension exceeds their unfolding threshold, generating turn-on fluorescence.

TGT probes were assembled as previously reported[55]. The TGT probes were assembled in 1 M NaCl by mixing the bottom strands (1 μM) and quencher strand (2 μM) in the ratio of 1:2 (Supplementary Table 2). The solution was heat annealed at 95 °C for 5 min and cooled down to 25 °C for 30 min.

The as-prepared $CaCO_3$ templates were dispersed in HEPES-buffered solution (pH = 6.5) containing HA-NH_2 (2 mg/mL) and assembled TGT probe (500 nM). After 1 h of agitation, HA/TGT-coated templates were collected via centrifugation (120 × *g*, 3 min), washed with HEPES (10 mM, pH 6.5), and resuspended in PEG-bis(*N*-succinimidyl succinate) solution (2 mg/mL in 10 mM HEPES, pH = 6.5). Following 4 h of agitation at 4 °C, crosslinked HA/TGT-coated templates were collected. $CaCO_3$ cores were dissolved with EDTA, yielding TGT-functionalized polysaccharidosomes subsequently modified with TLR agonists.

Mechanical and surface roughness characterization by atom force microscopy (AFM)

AFM imaging and force measurements were conducted using a BioFastScan scanning probe microscope (Bruker). AFM force measurements were conducted in liquid under ambient conditions. The polysaccharidosomes or Art-P cell suspensions were added dropwise and fixed onto a polylysine-coated glass coverslip. Commercially available AFM ball tips with a radius of 6 μm were used (spring constant of 0.1 N/m, deflection sensitivity of 37 nm/V). The results obtained from AFM were processed by NanoScope Analysis (Bruker) software, and the Young's modulus was calculated by fitting the data with the Hertzian model.

AFM imaging and roughness characterization were conducted in PeakForce Tapping mode in the air under ambient conditions. The polysaccharidosomes or Art-P cells were added dropwise onto a freshly cleaved silica surface and air-dried. The commercially available AFM cantilever tips were used and the scanning rate was set at 0.8 Hz. Raw height images were flattened using a first-order polynomial fit in Bruker NanoScope Analysis v1.9 software to remove tilt artifacts. Surface roughness parameters, including root-mean-square roughness (Rq), average roughness (Ra), and maximum height (Rmax), were calculated from at least three non-overlapping regions per sample with dimensions of 5×5 μm^2. The Ra of at least 30 tested surfaces were calculated for further analysis.

Cell culture and inhibitor treatment

Macrophages from the RAW 264.7 cell lines (from ATCC), THP-1 cell lines (from GeneChem), and primary BMDMs of mice (from QuiCell) were cultured with polysaccharidosomes or Art-P cells in a ratio of 5:1 for all cell experiments. RAW and BMDM cells were grown in DMEM medium that was supplemented with 10 vol% heat-inactivated fetal bovine serum and 1 vol% penicillin-streptomycin in a humidified chamber maintained at 37 °C under a 5% CO_2 atmosphere.

THP-1 cells were grown in RPMI-1640 medium that was supplemented with 10 vol% heat-inactivated fetal bovine serum and 1 vol% penicillin-streptomycin in a humidified chamber maintained at 37 °C

under a 5% CO_2 atmosphere. To induce macrophage differentiation, cells were treated with phorbol 12-myristate 13-acetate (100 ng/mL, MedChemExpress) in culture medium for 24 h.

hCD44 knockout THP-1 cell line was purchased from GeneChem (Catalog No. CGKO-M2393). Piezo1 knockout RAW 264.7 cell line was purchased from Cyagen (Catalog No. SY-KO-00329). Briefly, gRNA targeting the human *CD44* or mouse *Piezo1* exons was designed and constructed according to gene sequences obtained from NCBI. The synthetic gRNA was incubated with Cas9 protein and transfected into THP-1 or RAW264.7 cells using electroporation. Single cells were plated in 96-well plates and cultured in the prepared medium. When the confluence of cell clones generally reached 60%, the backup plating was performed. Extracted the DNA and amplified by PCR using the primers upstream and downstream of the gRNA target site and sequenced the amplified products to select the homozygous knockout clones. Cultivated homozygous knockout clones and extracted protein for validation of knockout at the protein level. Homozygous *hCD44* −/− THP-1 cell and homozygous *Piezo1* −/− RAW264.7 cell were obtained.

During the inhibitor experiments, the Latrunculin A (100 nM, Cayman, No. 10010630), Y27632 (10 μM, Yuanye Bio-Technology), or Yoda1 (1 μM, 5 μM, and 15 μM, Absin) was added during the whole cell culturing period.

RNA Isolation and RT-qPCR

Macrophages were co-cultured with polysaccharidosomes or Art-P cells with or without related inhibitors for 10 h, after which the cells were harvested and RNA immediately extracted. Total RNA was extracted from stimulated macrophages using an AxyPrep Multisource Total RNA Miniprep Kit following the manufacturer's instructions. The integrity of RNA was determined via spectrophotometric analysis of each sample at 260 and 280 nm. Samples were considered sufficiently pure if their 260/280 readings were 1.9–2.1. Complementary cDNA was synthesized using the SuperScript™ III First-Strand Synthesis System manufactured by Thermo Fisher® Scientific as per the manufacturer's instructions. Gene expression was analyzed via RT-qPCR using cDNA synthesized from extracted RNA as a template after co-culturing had been performed for 10 h. RT-qPCR was performed with a StepOnePlus® thermal cycler (Applied Biosystems), using the PowerUp® SYBR green Master mix and custom gene-specific primers for the genes of interest (Supplementary Table 1, purchased from Sangon Biotech). GAPDH was used as the endogenous or housekeeping gene. Relative quantification of transcript abundance was performed using the *ΔΔCt* method, and the threshold cycle (Ct) was obtained using the software LightCycler 96 SW 1.1 (Light Cycler 96 real-time PCR machine, Roche, Switzerland).

Cell surface CD86 detection

Macrophages were co-cultured with polysaccharidosomes or Art-P cells with or without related inhibitors for 24 h, after which the samples were collected in round-bottom tubes and washed with flow cytometry staining buffer (Thermo Fisher® Scientific, Cat. No. 00-4222). Non-specific Fc-mediated interactions were blocked by pre-incubating the samples with 0.5 μg CD16/CD32 Monoclonal Antibody (93) (eBioscience) in 100 μL (for 10^6 cells) at room temperature for 20 min. An equal volume of 50 μL of cell suspension (10^6 cells) was added to each tube and 0.06 μg of CD86 (B7-2) monoclonal antibody (GL1), APC (eBioscience, 50 μL) were mixed and added to the cells to give a final stain volume of 100 μL. After 40 min of incubation on ice, the samples were washed by flow cytometry staining solution three times using a centrifuge (500 x g, 5 min). The samples were resuspended in flow cytometry staining solution and were analyzed by flow cytometry.

Nitric oxide (NO) detection

Macrophages were co-cultured with polysaccharidosomes or Art-P cells with or without related inhibitors for 24 h, after which the culture medium was collected and the insoluble particles and cells were removed by centrifuge (500 × *g*, 5 min). The nitrite formed by the spontaneous oxidation of NO under physiological conditions was detected by the Griess Reagent Kit (Beyotime Biotechnology, S0021S) as per the manufacturer's instructions.

Immunofluorescence

The macrophages were grown on a high-affinity confocal cell culture dish. After 24 h of co-culturing, the samples were washed twice with phosphate-buffered saline (PBS) and then fixed with 4 vol% paraformaldehyde at room temperature for 30 min. The samples were then washed with cold PBS three times. Cells were permeated and non-specific antibody binding was blocked by incubating samples with Immunol Staining Blocking Buffer (Beyotime Biotechnology, P0102) for 60 min at room temperature. Subsequently, the samples were washed briefly with immunostaining washing solution (Beyotime Biotechnology, P0106C) and incubated overnight with primary antibodies at 4 °C. After the above process, the samples were washed twice with the washing solution and then incubated with secondary antibodies, 4′,6-diamidino-2-phenylindole (DAPI), and fluorophore-labeled phalloidin at room temperature for 60 min, then washed twice with washing solution.

The primary and secondary antibodies along with the corresponding concentrations used were NF-kappaB p65 (D14E12) XP® Rabbit mAb (Cell Signaling, 8242S, 1:1000 dilution); Mouse Monoclonal PIEZO1 Antibody (2–10) (Novus, NBP2-75617, 1:1000 dilution); CD44 Monoclonal Antibody (IM7) (eBioscience, 14-0441-82, 1:500 dilution); Ezrin/Radixin/Moesin Rabbit pAb (ABclonal, A21093, 1:250 dilution); RhoA (67B9) Rabbit mAb (Cell Signaling, 2117S, 1:500); Anti-rabbit IgG (H + L), F(ab′) $_2$ Fragment (Alexa Fluor ® 647 Conjugate, Cell Signaling, 4414S, 1:1000 dilution); TRITC phalloidin (Yeasen, 40734ES75, 1:100 dilution); Phalloidin-iFluor® 405 Conjugate (AATbio, 23111), Cy3-labeled Goat Anti-Rat IgG(H + L) (Beyotime, A0507, 1:500), Alexa Fluor 555-labeled Donkey Anti-Rabbit IgG(H + L) (Beyotime, A0453, 1:500), and Alexa Fluor 647-labeled Goat Anti-Mouse IgG (H + L) (Beyotime Biotechnology, A0473, 1:500 dilution).

Transmission electron microscope (TEM) characterization

After 24 h of co-culturing treatment, cells were fixed with glutaraldehyde and OsO_4, stained, dehydrated in a graded acetone series, infiltrated with Durcupan resin, and incubated at 60 °C for 48 h. The cell-embedded resin was then cut into sections with thicknesses of approximately 50 nm for TEM observation.

Calcium imaging

RAW 264.7 macrophages were grown in a confocal cell culture dish. The culture medium was removed, and the cells were washed three times with PBS. Subsequently, 1 mL of 4 μM Fluo-4, AM (Damas life) dissolved in PBS containing Pluronic F-127 (0.02 vol%) was added to the cells, followed by incubation at 37 °C for 30 min. Afterward, the cells were washed with PBS and incubated for an additional 25 min before co-culture treatment. Following a 30-min co-culture period, images of the samples were captured using a confocal microscope with an excitation wavelength of 488 nm.

Actin anisotropy quantification

Actin anisotropy was quantified in the maximum projection images from confocal stacks labeled with phalloidin. The anisotropy quantification was implemented using the ImageJ FibrilTool plug-in[89].

Fluorescence lifetime imaging microscopy (FLIM)

THP-1 macrophages were seeded in a confocal cell culture dish. After 12 h of co-culturing with PBS (control group) or Art-P cells under specified conditions, cells were thrice washed with PBS and treated with 1 μM of Flipper-TR® probe (Spirochrome, CY-SC020) in serum-

free RPMI-1640 for 15 min at 37 °C according to the manufacturer's protocol. Cells were washed once more with PBS, and RPMI-1640 was added to the cells. FLIM imaging was performed using single-molecule time-resolved confocal microscopy (PicoQuant, MicroTime 200). Excitation was performed using a pulsed 485 nm laser operating at 20 MHz, and the emission signal was collected through a 600/50 nm bandpass filter. SymPhoTime 64 software (PicoQuant) was then used to extract lifetime information, the photon histograms from regions of interest were fitted with a double exponential, and two decay times, τ1 and τ2, were extracted. The longest lifetime with the higher fit amplitude τ1 is used to report membrane tension.

Rho activation measurement

The level of active RhoA was determined using the G protein-linked (G-Lisa) assay kit (Cytoskeleton, BK124) by the manufacturer's protocol. Briefly, after co-culturing cells with PBS (control group) or Art-P cells under specified conditions for 30 min, the cells were washed with ice-cold PBS and lysed using the provided lysis buffer on ice. Protein concentration was measured and equalized to 0.5 mg/mL, and the samples were snap-frozen in liquid nitrogen. Triplicate assays were done, and the amount of active RhoA was measured at an absorbance of 490 nm as per the manufacturer's instructions.

Statistics and reproducibility

GraphPad Prism 9 was used for statistical analysis. All results are expressed as mean ± standard deviation. Two groups were compared by two-tailed Student's *t*tests, and multiple groups were compared by one-way analysis of variance (ANOVA) with Tukey-Kramer post hoc tests. Significance was demonstrated by $p < 0.05$ (ns, $p > 0.05$; *$p < 0.05$; **$p < 0.01$; ***$p < 0.001$; ****$p < 0.0001$). The experiment was repeated at least three times independently with similar results.

Reporting summary

Further information on research design is available in the Nature Portfolio Reporting Summary linked to this article.

Data availability

All data supporting the findings of this study are available within the paper and its Supplementary Information, or upon request from the corresponding authors. Source data are provided as a source data file.

Code availability

FibrilTool, an open-source image processing and analysis package, can be obtained from: http://rsbweb.nih.gov/ij/download.html.

References

1. Wang, N., Tytell, J. D. & Ingber, D. E. Mechanotransduction at a distance: mechanically coupling the extracellular matrix with the nucleus. *Nat. Rev. Mol. Cell Biol.* **10**, 75–82 (2009).
2. Humphrey, J. D., Dufresne, E. R. & Schwartz, M. A. Mechanotransduction and extracellular matrix homeostasis. *Nat. Rev. Mol. Cell Biol.* **15**, 802–812 (2014).
3. Sun, Q., Wei, Q. & Zhao, C. How do the cells sense and respond to the microenvironment mechanics?. *Chin. Sci. Bull.* **66**, 2303–2311 (2020).
4. Hui, Y. et al. Nanoparticle elasticity regulates phagocytosis and cancer cell uptake. *Sci. Adv.* **6**, eaaz4316 (2020).
5. Xie, W. et al. Static and dynamic: Evolving biomaterial mechanical properties to control cellular mechanotransduction. *Adv. Sci. (Weinh.)* **10**, e2204594 (2023).
6. Hui, Y. et al. Role of nanoparticle mechanical properties in cancer drug delivery. *ACS Nano* **13**, 7410–7424 (2019).
7. Saraswathibhatla, A., Indana, D. & Chaudhuri, O. Cell-extracellular matrix mechanotransduction in 3D. *Nat. Rev. Mol. Cell Biol.* **24**, 495–516 (2023).
8. Mittelheisser, V. et al. Evidence and therapeutic implications of biomechanically regulated immunosurveillance in cancer and other diseases. *Nat. Nanotechnol.* **19**, 281–297 (2024).
9. Plodinec, M. et al. The nanomechanical signature of breast cancer. *Nat. Nanotechnol.* **7**, 757–765 (2012).
10. Huang, Y. X. et al. Human red blood cell aging: Correlative changes in surface charge and cell properties. *J. Cell Mol. Med* **15**, 2634–2642 (2011).
11. Odermatt, P. D. et al. Overlapping and essential roles for molecular and mechanical mechanisms in mycobacterial cell division. *Nat. Phys.* **16**, 57–62 (2020).
12. Sun, Q. et al. Curved nanofiber network induces cellular bridge formation to promote stem cell mechanotransduction. *Adv. Sci. (Weinh.)* **10**, e2204479 (2023).
13. Wong, S. H. D. et al. Anisotropic nanoscale presentation of cell adhesion ligand enhances the recruitment of diverse integrins in adhesion structures and mechanosensing-dependent differentiation of stem cells. *Adv. Funct. Mater.* **29**, 1806822 (2019).
14. Liu, W. et al. Topographic cues guiding cell polarization via distinct cellular mechanosensing pathways. *Small* **18**, 2104328 (2021).
15. Changede, R., Cai, H., Wind, S. J. & Sheetz, M. P. Integrin nanoclusters can bridge thin matrix fibres to form cell-matrix adhesions. *Nat. Mater.* **18**, 1366–1375 (2019).
16. Wang, Z. et al. Snake venom-defined fibrin architecture dictates fibroblast survival and differentiation. *Nat. Commun.* **14**, 1029 (2023).
17. Wynn, T. A., Chawla, A. & Pollard, J. W. Macrophage biology in development, homeostasis and disease. *Nature* **496**, 445–455 (2013).
18. Mosser, D. M. & Edwards, J. P. Exploring the full spectrum of macrophage activation. *Nat. Rev. Immunol.* **8**, 958–969 (2008).
19. Wattrus, S. J. et al. Quality assurance of hematopoietic stem cells by macrophages determines stem cell clonality. *Science* **377**, 1413–1419 (2022).
20. Monks, C. R. F., Freiberg, B. A., Kupfer, H., Sciaky, N. & Kupfer, A. Three-dimensional segregation of supramolecular activation clusters in T cells. *Nature* **395**, 82–86 (1998).
21. Brown, A. C. N. et al. Remodelling of cortical actin where lytic granules dock at natural killer cell immune synapses revealed by super-resolution microscopy. *PLoS Biol.* **9**, e1001152 (2011).
22. Stinchcombe, J. C., Bossi, G., Booth, S. & Griffiths, G. M. The immunological synapse of CTL contains a secretory domain and membrane bridges. *Immunity* **15**, 751–761 (2001).
23. Natkanski, E. et al. B cells use mechanical energy to discriminate antigen affinities. *Science* **340**, 1587–1590 (2013).
24. Jain, N. & Vogel, V. Spatial confinement downsizes the inflammatory response of macrophages. *Nat. Mater.* **17**, 1134–1144 (2018).
25. Atcha, H. et al. Mechanically activated ion channel Piezo1 modulates macrophage polarization and stiffness sensing. *Nat. Commun.* **12**, 3256 (2021).
26. Bae, G. et al. Immunoregulation of Macrophages by Controlling Winding and Unwinding of Nanohelical Ligands. *Adv. Funct. Mater.* **31**, 2103409 (2021).
27. Kim, S. Y. et al. Modulation of Macrophages by In Situ Ligand Bridging. *Adv. Funct. Mater.* **33**, 2215166 (2023).
28. Vorselen, D. et al. Microparticle traction force microscopy reveals subcellular force exertion patterns in immune cell-target interactions. *Nat. Commun.* **11**, 20 (2020).
29. Doyle, A. D. & Yamada, K. M. Mechanosensing via cell-matrix adhesions in 3D microenvironments. *Exp. Cell Res* **343**, 60–66 (2016).

30. Liu, Y., Galior, K., Ma, V. P.-Y. & Salaita, K. Molecular Tension Probes for Imaging Forces at the Cell Surface. *Acc. Chem. Res* **50**, 2915–2924 (2017).
31. Mukwaya, V. et al. Lectin-glycan-mediated nanoparticle docking as a step toward programmable membrane catalysis and adhesion in synthetic protocells. *ACS Nano* **14**, 7899–7910 (2020).
32. Marcotti, S., Maki, K., Reilly, G. C., Lacroix, D. & Adachi, T. Hyaluronic acid selective anchoring to the cytoskeleton: An atomic force microscopy study. *PLoS ONE* **13**, e0206056 (2018).
33. Cywes, C., Stamenkovic, I. & Wessels, M. R. CD44 as a receptor for colonization of the pharynx by group A Streptococcus. *J. Clin. Invest* **106**, 995–1002 (2000).
34. Friedl, P., den Boer, A. T. & Gunzer, M. Tuning immune responses: diversity and adaptation of the immunological synapse. *Nat. Rev. Immunol.* **5**, 532–545 (2005).
35. Lvov, Y., Antipov, A. A., Mamedov, A., Möhwald, H. & Sukhorukov, G. B. Urease Encapsulation in Nanoorganized Microshells. *Nano Lett.* **1**, 125–128 (2001).
36. Khavani, M. et al. Effect of ethanol and urea as solvent additives on PSS-PDADMA polyelectrolyte complexation. *Macromolecules* **55**, 3140–3150 (2022).
37. Long, H., Vos, B. E., Betz, T., Baker, B. M. & Trappmann, B. Non-swelling and hydrolytically stable hydrogels uncover cellular mechanosensing in 3D. *Adv. Sci. (Weinh.)* **9**, e2105325 (2022).
38. Gupta, M. et al. Adaptive rheology and ordering of cell cytoskeleton govern matrix rigidity sensing. *Nat. Commun.* **6**, 7525 (2015).
39. Geng, J. et al. TLR4 signalling via Piezo1 engages and enhances the macrophage mediated host response during bacterial infection. *Nat. Commun.* **12**, 3519 (2021).
40. Davis, M. M. & Bjorkman, P. J. T-cell antigen receptor genes and T-cell recognition. *Nature* **334**, 395–402 (1988).
41. Long, E. O., Kim, H. S., Liu, D., Peterson, M. E. & Rajagopalan, S. Controlling natural killer cell responses: integration of signals for activation and inhibition. *Annu Rev. Immunol.* **31**, 227–258 (2013).
42. Li, J., Jiang, X., Li, H., Gelinsky, M. & Gu, Z. Tailoring materials for modulation of macrophage fate. *Adv. Mater.* **33**, e2004172 (2021).
43. Mukwaya, V. et al. Programmable membrane-mediated attachment of synthetic virus-like nanoparticles on artificial protocells for enhanced immunogenicity. *Cell Rep. Phys. Sci.* **2**, 100291 (2021).
44. Song, Y. et al. Transient nuclear deformation primes epigenetic state and promotes cell reprogramming. *Nat. Mater.* **21**, 1191–1199 (2022).
45. Hou, Y. et al. Surface Roughness and Substrate Stiffness Synergize To Drive Cellular Mechanoresponse. *Nano Lett.* **20**, 748–757 (2020).
46. Stowers, R. S. et al. Matrix stiffness induces a tumorigenic phenotype in mammary epithelium through changes in chromatin accessibility. *Nat. Biomed. Eng.* **3**, 1009–1019 (2019).
47. Wolf, K. J. et al. A mode of cell adhesion and migration facilitated by CD44-dependent microtentacles. *Proc. Natl. Acad. Sci. USA* **117**, 11432–11443 (2020).
48. Dalby, M. J., Gadegaard, N. & Oreffo, R. O. Harnessing nanotopography and integrin-matrix interactions to influence stem cell fate. *Nat. Mater.* **13**, 558–569 (2014).
49. Hirota, K. et al. Optimum conditions for efficient phagocytosis of rifampicin-loaded PLGA microspheres by alveolar macrophages. *J. Control Release* **119**, 69–76 (2007).
50. Miyake, K., Underhill, C. B., Lesley, J. & Kincade, P. W. Hyaluronate can function as a cell adhesion molecule and CD44 participates in hyaluronate recognition. *J. Exp. Med* **172**, 69–75 (1990).
51. Ponta, H., Sherman, L. & Herrlich, P. A. CD44: from adhesion molecules to signalling regulators. *Nat. Rev. Mol. Cell Biol.* **4**, 33–45 (2003).
52. Wang, X. & Ha, T. Defining single molecular forces required to activate integrin and notch signaling. *Science* **340**, 991–994 (2013).
53. Ma, V. P. & Salaita, K. DNA nanotechnology as an emerging tool to study mechanotransduction in living systems. *Small* **15**, e1900961 (2019).
54. Liu, Y. et al. DNA-based nanoparticle tension sensors reveal that T-cell receptors transmit defined pN forces to their antigens for enhanced fidelity. *Proc. Natl. Acad. Sci. USA* **113**, 5610–5615 (2016).
55. Hu, Y. et al. DNA-based microparticle tension sensors (muTS) for measuring cell mechanics in non-planar geometries and for high-throughput quantification. *Angew. Chem. Int Ed. Engl.* **60**, 18044–18050 (2021).
56. Wang, W. et al. Hydrogel-based molecular tension fluorescence microscopy for investigating receptor-mediated rigidity sensing. *Nat. Methods* **20**, 1780–1789 (2023).
57. Wisdom, K. M. et al. Matrix mechanical plasticity regulates cancer cell migration through confining microenvironments. *Nat. Commun.* **9**, 4144 (2018).
58. Gaertner, F. et al. WASp triggers mechanosensitive actin patches to facilitate immune cell migration in dense tissues. *Dev. Cell* **57**, 47–62 e49 (2022).
59. Biggs, M. J., Milone, M. C., Santos, L. C., Gondarenko, A. & Wind, S. J. High-resolution imaging of the immunological synapse and T-cell receptor microclustering through microfabricated substrates. *J. R. Soc. Interface* **8**, 1462–1471 (2011).
60. Mossman, K. D., Campi, G., Groves, J. T. & Dustin, M. L. Altered TCR signaling from geometrically repatterned immunological synapses. *Science* **310**, 1191–1193 (2005).
61. Moller, J., Luhmann, T., Chabria, M., Hall, H. & Vogel, V. Macrophages lift off surface-bound bacteria using a filopodium-lamellipodium hook-and-shovel mechanism. *Sci. Rep.* **3**, 2884 (2013).
62. Cavalcanti-Adam, E. A. et al. Cell spreading and focal adhesion dynamics are regulated by spacing of integrin ligands. *Biophys. J.* **92**, 2964–2974 (2007).
63. Fletcher, D. A. & Mullins, R. D. Cell mechanics and the cytoskeleton. *Nature* **463**, 485–492 (2010).
64. Elosegui-Artola, A. et al. Mechanical regulation of a molecular clutch defines force transmission and transduction in response to matrix rigidity. *Nat. Cell Biol.* **18**, 540–548 (2016).
65. Chan, C. E. & Odde, D. J. Traction dynamics of filopodia on compliant substrates. *Science* **322**, 1687–1691 (2008).
66. Borg, C. et al. NK cell activation by dendritic cells (DCs) requires the formation of a synapse leading to IL-12 polarization in DCs. *Blood* **104**, 3267–3275 (2004).
67. Verdijk, P. et al. Morphological changes during dendritic cell maturation correlate with cofilin activation and translocation to the cell membrane. *Eur. J. Immunol.* **34**, 156–164 (2004).
68. McWhorter, F. Y., Wang, T., Nguyen, P., Chung, T. & Liu, W. F. Modulation of macrophage phenotype by cell shape. *Proc. Natl. Acad. Sci. USA* **110**, 17253–17258 (2013).
69. Colom, A. et al. A fluorescent membrane tension probe. *Nat. Chem.* **10**, 1118–1125 (2018).
70. Park, J. S. et al. Mechanical regulation of glycolysis via cytoskeleton architecture. *Nature* **578**, 621–626 (2020).
71. Vorselen, D. Cell surface receptors TREM2, CD14 and integrin αMβ2 drive sinking engulfment in phosphatidylserine-mediated phagocytosis. *BioRixv* **50**, 1281–1291 (2022).
72. Jaumouille, V., Cartagena-Rivera, A. X. & Waterman, C. M. Coupling of beta(2) integrins to actin by a mechanosensitive molecular clutch drives complement receptor-mediated phagocytosis. *Nat. Cell Biol.* **21**, 1357–1369 (2019).
73. Solon, J., Levental, I., Sengupta, K., Georges, P. C. & Janmey, P. A. Fibroblast adaptation and stiffness matching to soft elastic substrates. *Biophys. J.* **93**, 4453–4461 (2007).

74. Engler, A. J. et al. Myotubes differentiate optimally on substrates with tissue-like stiffness: pathological implications for soft or stiff microenvironments. *J. Cell Biol.* **166**, 877–887 (2004).
75. Di, X. et al. Cellular mechanotransduction in health and diseases: From molecular mechanism to therapeutic targets. *Signal Transduct. Target Ther.* **8**, 282 (2023).
76. Ranade, S. S., Syeda, R. & Patapoutian, A. Mechanically activated ion channels. *Neuron* **87**, 1162–1179 (2015).
77. Douguet, D. & Honore, E. Mammalian mechanoelectrical transduction: Structure and function of force-gated ion channels. *Cell* **179**, 340–354 (2019).
78. Riento, K. & Ridley, A. J. Rocks: multifunctional kinases in cell behaviour. *Nat. Rev. Mol. Cell Biol.* **4**, 446–456 (2003).
79. Hall, A. Rho GTPases and the actin cytoskeleton. *Science* **279**, 509–514 (1998).
80. Discher, D. E., Janmey, P. & Wang, Y. L. Tissue cells feel and respond to the stiffness of their substrate. *Science* **310**, 1139–1143 (2005).
81. Schappe, M. S. et al. Chanzyme TRPM7 mediates the Ca (2+) influx essential for lipopolysaccharide-induced toll-like receptor 4 endocytosis and macrophage activation. *Immunity* **48**, 59–74 e55 (2018).
82. Bagaev, A. V. et al. Elevated pre-activation basal level of nuclear NF-kappaB in native macrophages accelerates LPS-induced translocation of cytosolic NF-kappaB into the cell nucleus. *Sci. Rep.* **9**, 4563 (2019).
83. von Erlach, T. C. et al. Cell-geometry-dependent changes in plasma membrane order direct stem cell signalling and fate. *Nat. Mater.* **17**, 237–242 (2018).
84. Wong, S. W., Lenzini, S., Cooper, M. H., Mooney, D. J. & Shin, J. W. Soft extracellular matrix enhances inflammatory activation of mesenchymal stromal cells to induce monocyte production and trafficking. *Sci. Adv.* **6**, eaaw0158 (2020).
85. Campas, O. et al. Quantifying cell-generated mechanical forces within living embryonic tissues. *Nat. Methods* **11**, 183–189 (2014).
86. Valastyan, S. & Weinberg, R. A. Tumor metastasis: Molecular insights and evolving paradigms. *Cell* **147**, 275–292 (2011).
87. Wang, Y., Kurum, A. & Tang, L. Soft cancer cells squeeze through T cell's grip. *Matter* **5**, 2510–2513 (2022).
88. Lei, K. et al. Cancer-cell stiffening via cholesterol depletion enhances adoptive T-cell immunotherapy. *Nat. Biomed. Eng.* **5**, 1411–1425 (2021).
89. Boudaoud, A. et al. FibrilTool, an ImageJ plug-in to quantify fibrillar structures in raw microscopy images. *Nat. Protoc.* **9**, 457–463 (2014).

Acknowledgements

We wish to gratefully acknowledge financial support from the Shanghai Science and Technology Plan Project (No. 25J22800600) to H.D., the National Key R&D Program of China (2022YFE0100600) to H.D., the National Natural Science Foundation of China (21871180 to H.D, 52150410403 to V.M.), the Tracking Program for Professor of Special Appointment (Eastern Scholar) at the Shanghai Institutions of Higher Learning (SHDP201802) to H.D., the Open Project of Translational Medicine of Shanghai Jiao Tong University (Nos. TMSK-2021-108, TMSK-2021-305) to H.D., Shanghai Jiao Tong University Translation Medicine Cross Research Fund (YG2021QN09) to H.D., STAR Program of Shanghai Jiao Tong University (No. 20240303) to H.D., and Shanghai Jiao Tong University 2030 Initiative. The authors also wish to thank the Instrumental Analysis Center (IAC) at Shanghai Jiao Tong University for providing measurements to support our experiments.

Author contributions

X. Y. and H. D. conceived the project. X. Y., V. M. and H. D. designed the experiments. X. Y., L. W. and W. Z. performed the experiments of the mechano-transduction between bone marrow-derived macrophages and Art-P cells, X. Y performed all rest experiments. X. Y., S. M. and H. D. wrote the manuscript.

Competing interests

The authors declare no competing interests.

Additional information

Supplementary information The online version contains supplementary material available at https://doi.org/10.1038/s41467-025-63581-1.

Correspondence and requests for materials should be addressed to Stephen Mann or Hongjing Dou.

Peer review information *Nature Communications* thanks Bo Huang and the other anonymous reviewer(s) for their contribution to the peer review of this work. A peer review file is available.